# Final Scientific Report - PUBLIC
# COVER PAGE

**Federal Agency to which Report is submitted:** DOE EERE – Wind & Water Power Program

**Recipient:** General Electric – Global Research, Niskayuna / DUNS No. 086188401
**Award Number:** DE-EE0005143
**Project Title:** Superconductivity for Large Scale Wind Turbines
**Project Period:** 09/30/2011 through 04/30/2012

**Principal Investigator:** Ruben Fair, Senior Electrical Engineer, fair@ge.com, 518 387 5279

**Date of Report:** 30th April 2012
**Covering Period:** 09/30/2011 through 04/30/2012
**Report Frequency:** Final

**Working Partners:** Robert Duckworth, Oak Ridge National Laboratory, duckworthrc@ornl.gov
**Cost-Sharing Partners:** Not applicable

**DOE Project Team:** DOE HQ Program Manager – Jose Zayas
DOE Field Contract Officer – Pamela Brodie
DOE Field Grants Management Specialist – Jane Sanders
DOE Field Project Officer – Nick Johnson
DOE/CNJV Project Monitor – Shaun Jensen

**Signature of Submitting Official: __Ruben Fair_____**
(electronic signature is acceptable)

## Acknowledgement:

This material is based on work supported by the Department of Energy under Award Number DE-EE0005143.

## Disclaimer:

## Additional Acknowledgements:

A significant number of individuals contributed to the work covered by this report. The individuals listed here are contributors to this project but have drawn broadly on the work from others in GE-Global Research, GE-Energy and Oak Ridge national Laboratory.

**GE-Global Research**

Mike Douglass
Wolfgang Stautner
Renuka Rajput-Ghoshal
Patrick Riley
Mike Moscinski
David Wagner
Joo Kim
Suyu Hou
Fulton Lopez
Randy Longtin
James Rochford
Trifon Laskaris
James Bray
Konrad Weeber
Probir Ghoshal
Kiruba Haran
Tsarafidy Raminosoa
Charles Stephens
Bob Zirin
Daniel Erno
Manoj Shah
Jim Alexander
Johanna Wellington
David Wardwell
Ann Agosti
Scott Quirion

**GE-Energy**

Adam Minadeo
Clive Lewis
Joseph Eugene
David Swaffield
Martin Ingles
Henning Marxen

**Oak Ridge National Laboratory**

Robert Duckworth

# Contents

**Project Objective:** The primary objective of the project is to apply low temperature superconducting technology to the design of a direct-drive wind turbine generator at the 10MW power level in order to reduce the Cost of Energy (COE).

**Project Goals:** Phase 1 of the project will focus on the design of the generator, an evaluation of the commercial viability of the design together with an identification of high risk components.

## Executive Summary

A conceptual design has been completed for a 10MW superconducting direct drive wind turbine generator employing low temperature superconductors for the field winding. Key technology building blocks from the GE Wind and GE Healthcare businesses have been transferred across to the design of this concept machine. Wherever possible, conventional technology and production techniques have been used in order to support the case for commercialization of such a machine. Appendices A and B provide further details of the layout of the machine and the complete specification table for the concept design.

Phase 1 of the program has allowed us to understand the trade-offs between the various sub-systems of such a generator and its integration with a wind turbine.

A Failure Modes and Effects Analysis (FMEA) and a Technology Readiness Level (TRL) analysis have been completed resulting in the identification of high risk components within the design.

The design has been analyzed from a commercial and economic point of view and Cost of Energy (COE) calculations have been carried out with the potential to reduce COE by up to 18% when compared with a permanent magnet direct drive 5MW baseline machine, resulting in a potential COE of 0.075 $/kWh.

Finally, a top-level commercialization plan has been proposed to enable this technology to be transitioned to full volume production.

The main body of this report will present the design processes employed and the main findings and conclusions.

# 1. SOPO Task Number 1 - Conceptual Design

## 1.1. SOPO Task Number 1.1 - Development of the optimal designs for GE's novel superconducting machine concept

### 1.1.1. Engineering Design Process

The overall engineering design process as applied to the design of our superconducting (SC) generator is outlined in this section and illustrated in Figure 1 below.

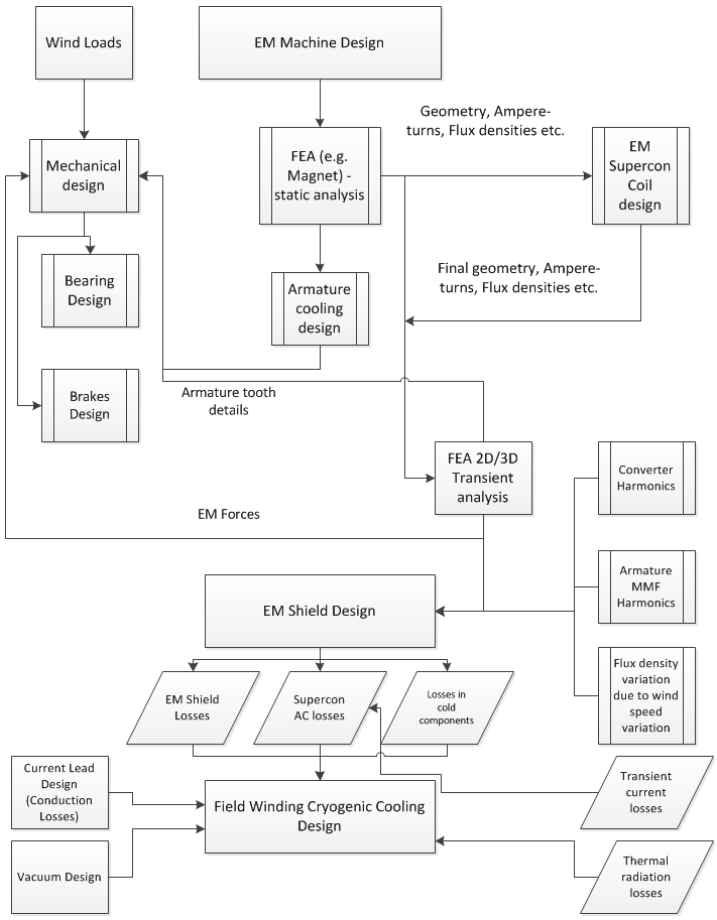


Figure 1 – Overall Engineering Design Process

The design starts with a preliminary electromagnetic (EM) machine design. Output from this design step is then used as input to the superconducting field coil design. The geometry of the machine, ampere-turns in the superconducting coils and required flux densities are then optimized. This optimized design is fed back into the generator EM design and the cooling for the armature windings is optimized. Transient analyses are performed on the complete machine and this feeds into the mechanical analysis and electromagnetic shield design steps. Additional inputs to the EM shield design include harmonics and wind load variations. Wind load is also a key input to the mechanical design which shapes the design for the shaft system, the bearings and the brakes. The EM shield design plays an important part in the determination of AC losses in the superconducting coils as well as transmitted losses to all the cryogenically cold components. These losses along with the current lead design and thermal radiation losses feed into the cryogenic cooling design for the superconducting field winding.

## 1.1.2. Generator Electromagnetic Design

A number of target design parameters related to size and rating were established as detailed in Table1 below. With input from the GE Wind business, the rated speed of rotation was set at 10 rpm. The rated voltage was selected to be 3300 V line-line based on the availability of an existing full power converter at that voltage in a similar rating, and the selected armature winding insulation system. The efficiency target was set at 95-96% based on comparison to other direct drive generators. The outside diameter of the superconducting field structure was set at 4.3 meters based on road shipping limits and the requirement to build this assembly in one piece.

Table 1 – Generator Final Design Parameters

| Parameter | Value |
|---|---|
| Rated Power | 10 MW |
| Rated Speed | 10 rpm |
| Rated Voltage | 3300 V line-line |
| Rated Current | 1750 A |
| Rated Power Factor | 1.0 |
| Full Load Efficiency | 95-96% |
| Armature Core Outer Diameter | 4.83 m |
| Armature Core Length | 1.88 m |
| Field Assembly Outer Diameter | 4.29 m |
| Physical Air gap length | 19 mm |
| No. of poles / No. of slots | 36 / 648 |
| Armature Winding Type | 3 phase, 2 layer, lap, form wound |
| Insulation | Class F (with Class B temperature rise) |
| SC Field MMF | 928000 AT/pole |
| Cooling | Axial air cooled thru air gap and yoke |

**Design Process**

The initial electromagnetic design process started by referring to work done at GE-GR in a 2006 study on an early direct drive 10 MW superconducting generator. In that study the generator was only sized electromagnetically. In the present study, the electromagnetic design was evolved to include the thermal, structural, and manufacturing constraints while minimizing weight and maintaining the generator electromagnetic performance.

Approximate electromagnetic designs were obtained by using a GE-GR in-house design tool originally written for permanent magnet field machines, and for this project, modified for superconducting field machines. This allowed rapid design iterations to be made, while exploring many different options. Key trade studies conducted using this tool were the choice of armature materials, the number of poles, and the armature dimensions. Initial field coil dimensions, MMF, and vacuum chamber and thermal shield dimensions and materials were provided by the superconducting coil design team. After a design was selected using the GE-GR tool, a commercially available finite element analysis design software package (MAGNET) was used to model the finer details and to analyze for machine performance. The MAGNET software, also confirmed results obtained from the in-house tool and from the superconducting magnet

design analysis. Following electromagnetic analysis, the design details were provided for a thermal analysis and manufacturing considerations. This process was iterated until all performance goals were met and weight was minimized.

The model used for finite element analysis is shown below. The model is two poles (1/18$^{th}$) of the generator and uses periodic symmetry. Static and time stepping rotation is used to calculate flux densities, forces, voltages, torques, and losses.

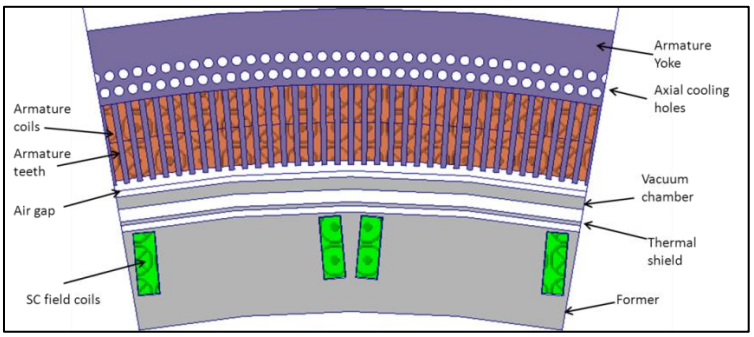


Figure 2 – Electromagnetic finite element model for the generator

**Number of Poles**

Generator pole number was studied and optimized for the lowest generator weight. The pole arc and subsequently the number of poles are important factors relating to the amount of leakage flux and hence the useful flux reaching the armature coils. Less flux requires a longer generator to maintain the same performance. Fewer poles increase the useful flux, but also the armature yoke thickness and end winding length. Ultimately, there is a tradeoff between armature weight due to the yoke thickness and end winding length resulting in an optimum choice of 36 poles for this application.

**Depth of Armature Slots**

Another trade study was the optimization of the depth of the armature slots. As the average distance between the armature coils and the superconducting field increases, the useful magnetic flux reaching the armature winding decreases. Deeper slots increase the winding copper, but reduce the useful flux. More copper improves efficiency and less useful flux decreases the efficiency. The armature slot depth was optimized for lowest generator weight with constant efficiency. A 5 inch slot depth was found to be optimum.

**Armature Teeth Material**

The most difficult trade was whether the armature core teeth should be magnetic iron or non-magnetic. Iron teeth are the traditional rotating machine configuration and draw more useful flux to the armature winding. Non-magnetic teeth reduce some of the negative effects of magnetic teeth, including losses induced in the field conducting components and torque and voltage ripple. Both design configurations were optimized and compared. Based on the pros and cons, the team down selected the iron teeth option primarily for the advantages of less complicated and lower cost construction. The magnetic teeth option selected included increasing the air gap to reduce the AC losses induced in conducting field components.

## Number of Armature Slots versus Losses

The early electromagnetic design had 9 slots/pole and 324 slots in total. With the distributed 2 layer winding this gave a typical armature coil size and a low armature space harmonic content. The AC loss in the armature windings of this type of superconducting generator tends to be higher due to the high magnetic saturation in the armature teeth. With 324 slots, the coil turns would have needed to be stranded to a very high degree to limit the AC loss. This would have meant increased manufacturing production costs and bespoke tooling to handle this non-standard coil construction. Another option for the armature coils would have been to construct the turns of Litz wire. This option is much more costly and would have reduced the slot copper fill, requiring an increase in generator size to maintain efficiency and thermal performance.

AC losses induced in the field assembly components are also affected by the number of armature slots. The vacuum chamber wall is the primary magnetic shield employed to limit these losses, but some loss will still be generated in the thermal shield and field winding former.

Further design iterations indicated that increasing the armature slots to 18 slots/pole and 648 slots in total was the ideal choice for the following reasons:

a) The resulting reduced armature coil width requires only 2 strands wide per turn to limit the AC loss to an acceptable level. This stranding using rectangular copper wire is producible using traditional manufacturing methods.

b) The increased number of slots also dramatically reduces the AC losses in the field parts. This reduction allows the vacuum chamber wall to be changed from copper to structural aluminum which is lower in cost and avoids the welding of dissimilar materials.

## Open Circuit Analysis

The no load magnetic flux density plot shows the very high flux densities resulting from the superconducting excitation field, even though the magnetic circuit is largely composed of non-magnetic materials. The armature teeth are driven well above their saturation density. The table highlights the flux densities in the main components and compares them to what would be typical in a conventional wound field or permanent magnet generator.

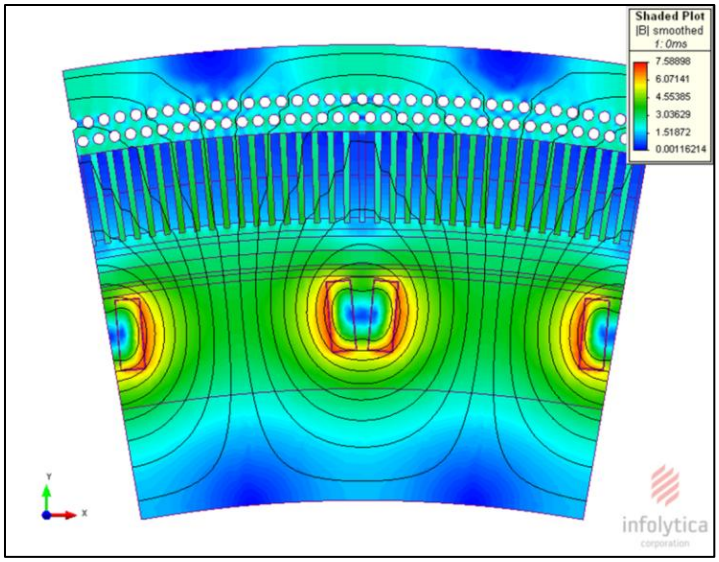

Figure 3 – Open Circuit Flux Density (Tesla)

Table 2 – Flux Density Comparison

| Component | 10 MW SC Generator | Conventional Generator | Avg. Increase With SC |
|---|---|---|---|
| Field Pole Center | 3.5 T | 1.5 – 2.0 T | 100% |
| Air Gap, peak | 2.6 T | 1.0 – 1.5 T | 110% |
| Armature Teeth | 3.0 – 3.4 T | 1.5 – 2.0 T | 80% |
| Armature Yoke | 2.5 T | 1.5 – 2.0 T | 40% |

The iron armature teeth produce a modulation of the air gap flux and results in an AC component in the open circuit voltage. A one slot skew of the armature core laminations along its axial length can be employed to smooth the voltage. Below is a plot of the voltages without and with skew.

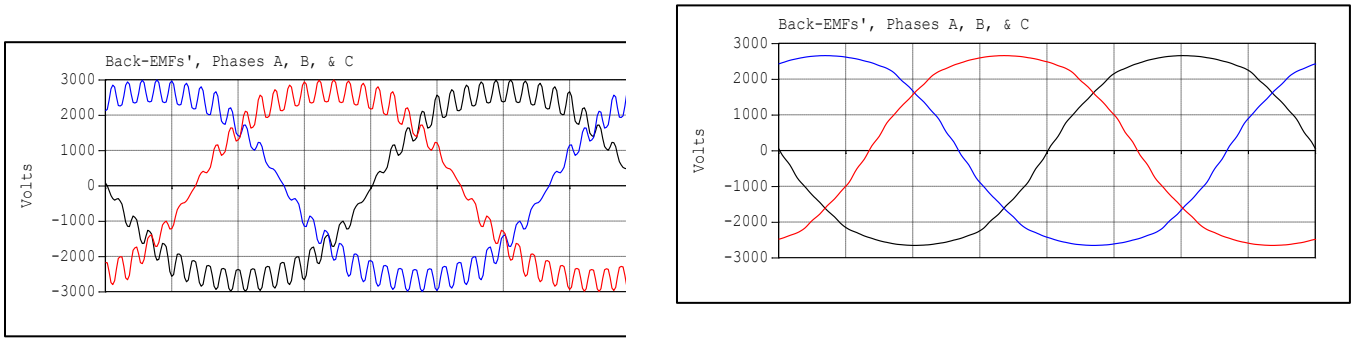


Figure 4 – Open circuit voltage – (a) without armature skew (b) armature skewed by one slot

## Full Load Analysis

The full load flux densities are very much the same as the no load described earlier because the magnetic field is relatively unaffected by generator full load currents.

The shaft torque corresponding to the voltage and currents is shown below. The torque ripple of about 2% represents a reduction from greater than 10% for an armature core without skewing.

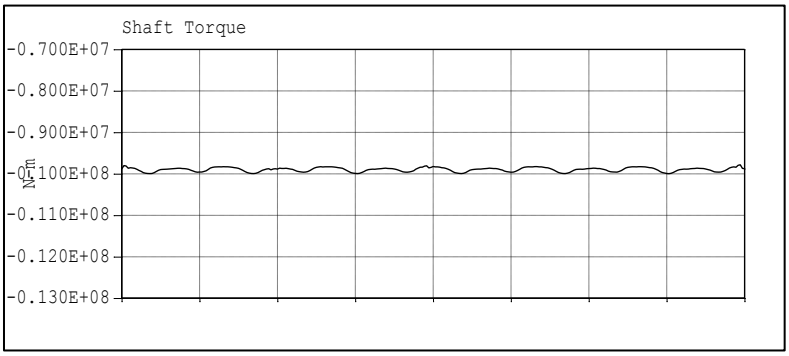


Figure 5 – Full Load Shaft Torque (Nm)

The torque shown is a function of the shear stress and surface area at the air gap of the generator. The shear stress is much higher in this generator compared to conventional generators due to the high magnetic flux density. The high shear stress correspondingly results in a higher torque density. Torque density is sometimes calculated from the electromagnetic (active) components only, meaning the basic winding and magnetic steel mass. Torque density can also be calculated using the entire generator or drive train mass. For this generator, guidance is given on which components to include in the drivetrain

mass. The following table shows the comparison of these figures of merit to a conventional state of the art permanent magnet direct drive wind generator.

Table 3 – Shear Stress and Torque Density Comparison

| Figure of Merit | 10 MW SC Generator | Conventional PM Generator | Increase with SC |
|---|---|---|---|
| Shear Stress | 179 kPa | 85 kPa | >100% |
| Torque Density (EM only) | 197 Nm/kg | 94 Nm/kg | >100% |
| Torque Density (Drivetrain) | 92 Nm/kg | 44 Nm/kg | >100% |

## Magnetic Forces on Generator Components

In addition to the tangential magnetic force at the air gap that produces the desired torque, the magnetic fields in the generator produce other forces on generator components. The net radial force on the rotor as a whole is zero for a uniform air gap. However with eccentricity of the armature to the field, a negative magnetic force results that tends to worsen the eccentricity. This force needs to be accounted for in the structural support of the generator armature and rotor as well as in the design of the generator bearings. The field superconducting coils also have radial and tangential forces under normal operation.

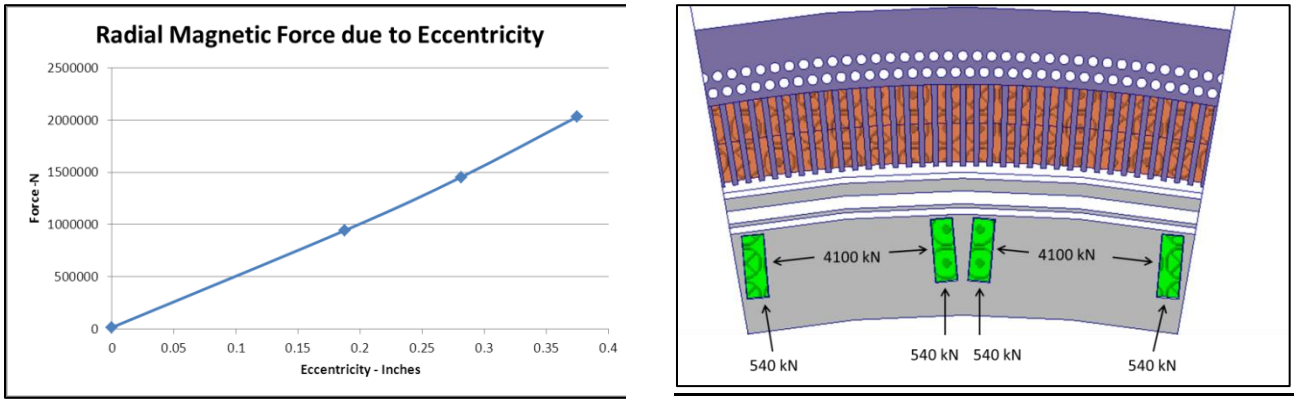


Figure 6 – Magnetic forces on generator components

(a) Radial magnetic force due to eccentricity (b) Forces on field coils

## Short Circuit Performance and Machine Reactances

Short circuit fault torques and currents are high for this type of superconducting generator design. The generator is sized for minimum weight consistent with good thermal performance. This results in excess electromagnetic capacity. Consequently the machine reactances that limit the fault currents are low compared to more conventional generators.

The peak short circuit current is 15 p.u. for a L-L-L short circuit, and 13 p.u. for a L-L short circuit. The peak short circuit torque is 10 p.u. for a L-L-L short circuit, and 12 p.u. for a L-L short circuit. Generator reactances compared to a conventional permanent magnet generator are shown in the following table.

Table 4 – Reactance Comparison

| Reactance | 10 MW SC Generator | Conventional PM Generator | SC / PM Gen Fault Currents |
|---|---|---|---|
| Xd (pu) | 0.09 | 0.7 | 8X |
| X"d (pu) | 0.07 | 0.4 | 6X |

## Transient Losses in the Field

Transient losses are induced in the conducting field components during armature short circuits, due to the high unbalanced armature currents. For sustained L-L-L and L-L short circuits, the losses induced in the vacuum chamber, thermal shield and former are shown as follows.

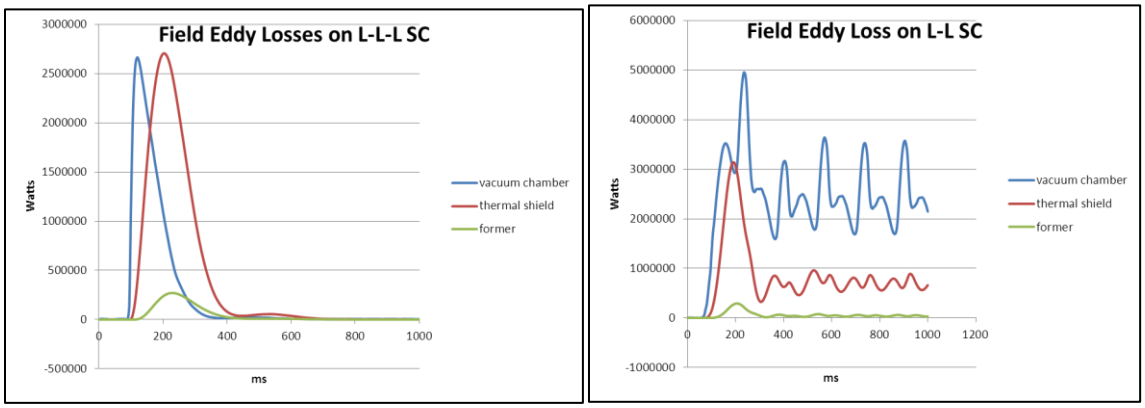


Figure 7 – Transient losses in the superconducting field assembly

These losses represent a very large heat load to the field and for a L-L short circuit the losses remain high for the duration of the short circuit. If these faults occur downstream of the protective devices, they would be interrupted in a short time and the field component masses would not experience an excessive temperature rise. However, if these faults occur in the generator winding or on the upstream side of the protective devices, the fault may not be quickly interrupted. Although a potentially rare occurrence, this particular fault phenomenon will nonetheless require further investigation.

## Discussion of fault mitigation and potential redesign

It would be very challenging to design the generator mechanical structure to withstand the peak levels of fault currents and torques. Currently the generator structure is designed for 3X rated torque. The fault protection methodology being considered is a set of fast acting circuit breakers and/or fuses to interrupt the fault current before the torque exceeds the 3X rated value. The fault torque curves indicate that the fault current would need to be interrupted within 5ms of the short.

In the event that protective devices cannot be sourced or developed to act fast enough to limit the torque to 3X rated, the generator design can be modified to reduce the fault current. One approach to a redesign would be to add more effective armature cooling, such as liquid cooling allowing the generator size and weight to be decreased along with the fault currents with a reduction in efficiency. Another approach would be to add more armature winding copper mass while decreasing the generator capacity. This approach would lower the fault currents at the expense of an increase in generator mass. The two approaches mentioned above could also be combined.

Although the fault scenarios described above are potentially rare occurrences, they will nonetheless require further investigation.

## Losses and Efficiency

By far, the largest loss and armature thermal driver is the armature winding DC loss which is defined as the $I^2R$ loss in the winding due to rated current and the DC winding resistance. The armature winding AC loss is the second most significant loss in the armature. It includes strand proximity, skin effect, and parallel strand circulating current losses. These losses are controlled by stranding of winding turns and transposing the turn half way through the coil. Losses in the armature core laminations and metal

structure are relatively low due to the very low fundamental frequency of 3 hertz. Losses induced at full load in the superconducting field conducting components are reasonable and do not exceed the cryocooling budget.

The loss summary and efficiencies for full and part loads are given in the following table.

Table 5 – Breakdown of generator losses

| Generator Load | 100% - 10MW | 50% - 5MW | 25% - 2.5MW |
|---|---|---|---|
| Turbine speed * | 10 rpm | 7.9 rpm | 6.3 rpm |
| Arm winding DC Loss | 363 kW | 144 kW | 57 kW |
| Armature AC Loss | 56 | 35 | 22 |
| Armature Yoke Loss | 5.7 | 4.5 | 3.6 |
| Armature Teeth Loss | 5.6 | 4.5 | 3.5 |
| Armature Core Clamp Loss | 2.1 | 1.3 | 0.8 |
| Field AC Loss | 2.6 | 2.1 | 1.6 |
| Armature Slip Ring Loss | 4.6 | 2.9 | 1.8 |
| Friction and Windage | negligible | negligible | negligible |
| Cryocooler power (3) | 22.5 | 22.5 | 22.5 |
| Cooling Air Blowers | (6) 39 | (4) 26 | (2) 13 |
| Total Loss | 501 kW | 243 kW | 126 kW |
| Efficiency | 95.2% | 95.4% | 95.2% |

*****$Generator\ power\ is\ assumed\ to\ be\ proportional\ to\ the\ rpm\ to\ the\ 3^{rd}\ power$

## 1.1.2.1. Generator Armature Slip Ring Design

The concept of the rotating armature requires current collector rings to transfer the three phase power through brushes to the stationary power convertors. These types of current collectors are common in the exciter systems of hydro-generators operating at speeds of about 100rpm and have brush lives of over a year. This translates to a brush-life of more than five years for our generator concept which operates at a speed of 10rpm.

GE has long industrial experience designing and manufacturing these high power current collectors and has successfully operated a 100MVA brush system for a variable frequency transformer (VFT) since 2007 with a high level of reliability. The VFT used a 3 phase, 3500A, 17kV, 100MW slip ring/collector system and the Performance Factor (PF) after 3 years of commercial operation was measured to be 99.7% which is an equivalent of 3.28 days outage out of a total of 1095 days operation.

A summary of the key parameters of the slip ring/collector system for our concept generator design is shown in the table below.

Table 6 – 10 MW rated armature slip rings

| Parameter | Value |
|---|---|
| No. of slip rings | 4 |
| Slip ring material | Steel |
| Slip ring outer diameter | 3 m |
| No. of carbon brushes per slip ring | 30 |
| Current per brush | 60 A |
| Rotational speed | 10 rpm |
| Brush wear per year | less than 2mm @ 10 rpm |
| Total operational loss @ 10MW | 4.6kW |

A further possibility being considered to reduce cost and up-tower weight would be to use commutating slip rings to feed DC to the convertor. This could lead to additional convertor cost and weight savings.

## 1.1.2.2. Generator Armature Cooling Design

The key thermal constraint was to limit the hot spot temperature for the armature winding to no more than 130$^{o}$C, corresponding to a Class B insulation temperature rise for the Class F insulation system proposed. This is standard practice to prolong the insulation life for rotating machines. However, considering that a wind turbine (even for off-shore systems) may spend a proportion of its time at part load, this suggests that aiming for a higher hot spot temperature, say 155$^{o}$C which is consistent with Class F insulation, may provide an opportunity to relax the cooling requirements allowing for a greater measure of redundancy when selecting air blowers without compromising winding insulation life.

Although water cooling of the armature for a slow rotating generator (10 rpm) may be easier to achieve than for a faster turning machine, air cooling was selected to reduce the complexity of the system and to keep overall costs low.

**Design Process**

The cooling design process is composed of three main steps and is described in the figure below. The first step is to identify critical design data from the generator electrical design output file. This step involves converting loss data into heat generation densities and building a simplified 2-D geometry for the armature yoke, copper coils and teeth. Secondly, the cooling channel configurations are included in the 2-D thermal model. The boundary conditions (BCs) such as heat transfer coefficients for the various working fluids and effective thermal conductivities for the various materials are then calculated. Pressure drops across the armature are also estimated at this stage to size the air-blowers. In the final step, after applying the required boundary conditions and thermal inputs to the 2-D FEA thermal model, the temperature profile for the armature can be calculated to identify the hotspot temperature and its location. A few inputs such as the cooling channel configuration and heat transfer coefficients can be iterated to meet the temperature limit requirement for the armature winding insulation.

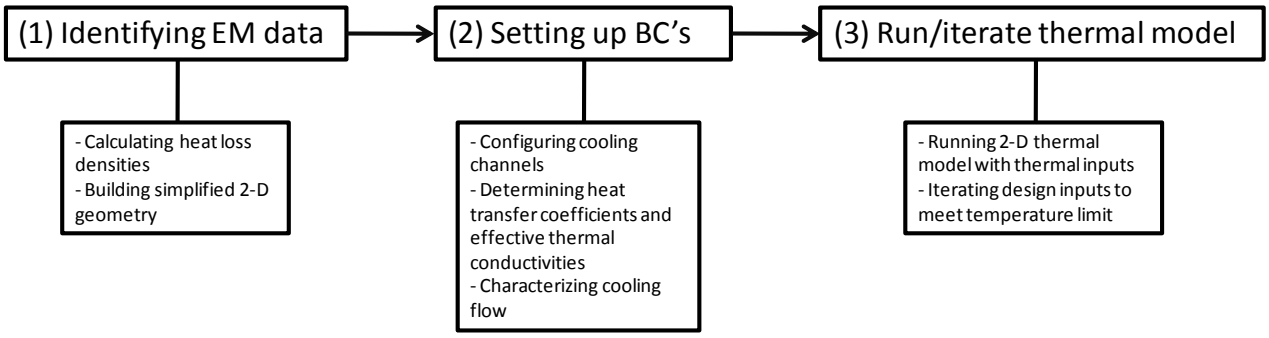


Figure 8 – Armature cooling design process

Aerovent centrifugal fans were selected for the air-blowers and analyzed in terms of flow rate capability at a given system pressure drop. The overall cooling flow rate was determined by the number of blowers and the system pressure drop. Based on the geometry of the cooling channel and airgap dimensions, flow distribution of the air flow through the armature's cooling channels and through the airgap are determined and heat transfer coefficients are estimated. The calculated value for the heat transfer coefficient for the armature cooling channels was further reduced to account for the presence of resin from the vacuum pressure impregnation (VPI) process applied to the armature winding and core.

**Magnetic vs. Non-magnetic teeth**

2-D thermal analyses for the axial cooling design were carried out to compare the thermal performance of armature designs with magnetic teeth and non-magnetic teeth as shown below. The hot spot temperature for the armature winding for the magnetic teeth option was about 130.5°C while that for the non-magnetic option was about 1.9°C higher.

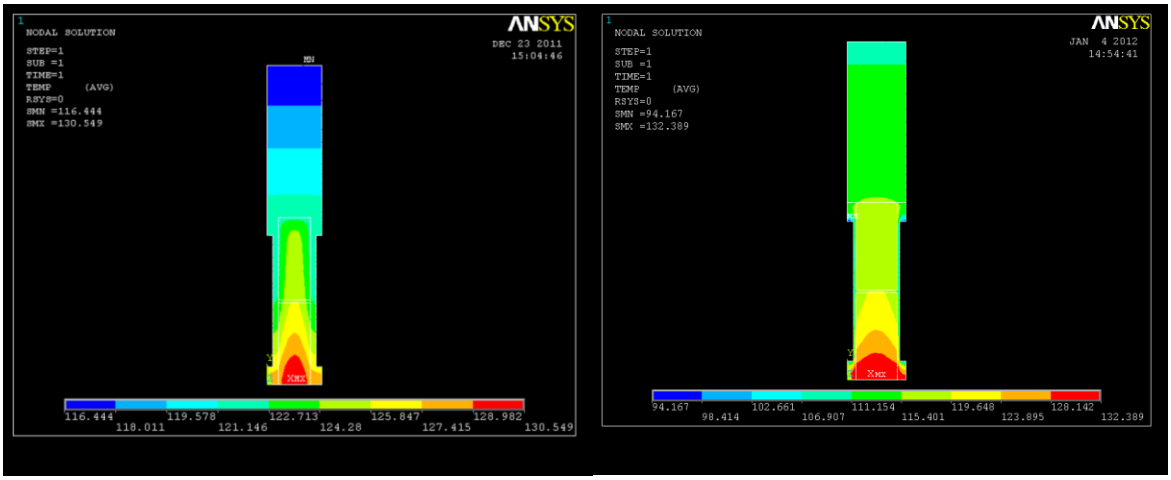


*(a) Magnetic teeth* *(b) Non-magnetic teeth*

Figure 9 – Armature hotspot comparison for magnetic vs. non-magnetic teeth

An additional 2-D thermal analysis was conducted for the outer vacuum chamber wall of the superconducting field winding assembly which is located within the generator's airgap. Due to the proximity of the iron teeth of the armature to this vacuum chamber wall and the slot/tooth passing frequency during rotation of the armature, eddy currents and thus losses are induced in the wall of this vacuum chamber. The rotation of the armature generated ~8kW of heat loss within this chamber wall. The temperature of the vacuum chamber wall needs to be maintained below ~80°C in order to minimize the thermal radiation heat load onto the cryogenically cold components located within the vacuum chamber. The hotspot temperature for the vacuum chamber wall was calculated to be 47.2°C with non-magnetic teeth and 48.2°C for the magnetic teeth design. These hotspot temperatures are well below the thermal radiation limit (80°C) described above, and therefore will have no detrimental effect on the radiation heat load onto the field winding assembly.

**Axial vs. Radial cooling**

Radial armature ducts with reverse/forward flow are known to require higher fan power to operate and have a more complex construction compared to an axial flow scheme. However, radial cooling has an advantage over axial cooling when the cooling gas is at atmospheric pressure because of the lower exit-air temperature.

*(a) Single-ended radial cooling* *(b) Single-ended axial cooling*

Figure 10 - Cooling schemes considered

Single-ended radial cooling (see figure above) has an issue (compared to double-ended radial cooling) in that there could be a lack of cooling flow near the exit as the majority of the total cooling flow would be vented to the radial channels before the cooling flow reaches the exit section - due to the pressure drop across the air gap.

Axial cooling was selected for the generator to avoid the issues described above and additionally to eliminate a risk of flow blockage due to the narrow armature teeth and airgap employed in the machine design.

**Final selected cooling design for 648 slots design with 0.75 inch airgap**

For the 648-slot design, the tooth width at the armature bore is only 0.327 inch, which means it is not practical to locate any cooling channels within the tooth area. Additionally, placing the cooling channels in the tooth region is more challenging due to the presence of the clamping fingers used to compress the armature lamination stack. The air cooling holes were therefore moved to the yoke area (i.e.back of armature core) as shown in below.

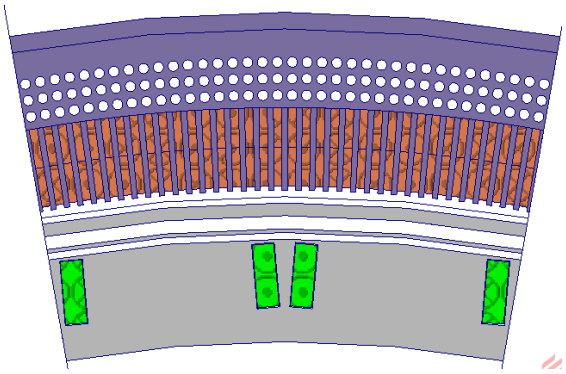

Figure 11 – 648 slots armature with 3 rows of cooling holes in the yoke

A series of two and three rows of 0.625 inch diameter cooling holes in the yoke area were analyzed while varying the number of air blowers to satisfy the thermal hot spot requirement of 130$^{o}$C. The final design for the cooling of the armature settled upon 2 rows of cooling holes with a total of 6 air-blowers providing a more uniform air flow distribution and a measure of redundancy. For Class F insulation, the allowable hot spot temperature is actually 155$^{o}$C, thus allowing for the failure of up to 2 blowers as indicated in the following table.

Table 7 – Blower redundancy check

| No. of working blowers | Armature Hotspot |
|---|---|
| 6 | 133 $^{o}$C |
| 5 | 145.7 $^{o}$C |
| 4 | 157.2 $^{o}$C |

**Air blower location**

Further analysis showed that there were two key advantages in moving the blowers from their previous position above the field winding assembly to just below the assembly. The new blower positions located on the field support plate. Firstly, this means that air-baffles and brush seals are no longer required. Secondly, the hub end has a natural curvature and angle allowing the air flow path to turn 180 degrees to flow into the armature axial cooling holes and the air gap space before exiting at the non-hub end. This air would then be cooled either by a water/air or air/air heat exchanger before being returned to the machine. The annulus where the air flows (i.e. below the field winding assembly) is about two times larger than the area of the air gap plus the cooling holes.

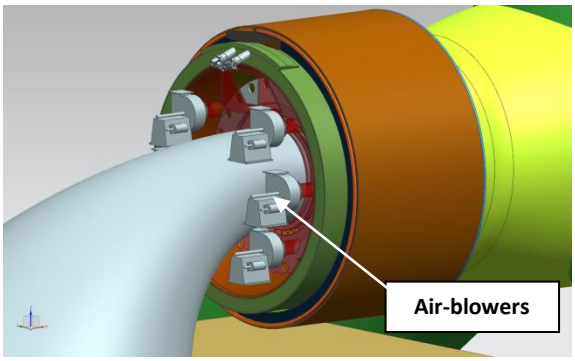


Figure 12 – Air blower location

The estimated pressure drop increase (or blower input power increase) due to the new location for the blowers turns out to be only 4.4% which is well within the capability of the selected air-blowers.

### 1.1.2.3. Power Convertor

Our direct drive generator will require a full power convertor connecting the armature to the grid. Selection of the appropriate convertor bridge topology plays an essential part in the overall reliability of the drivetrain. Current harmonics can cause extra losses in the generator windings and this usually results in a higher rated generator design. Torque harmonics can also sometimes be experienced by the shaft connected to the wind turbine rotor. For variable speed operation and especially for slow turning generators such as our concept design both 6-pulse and 12-pulse diode-bridge convertors can exacerbate these harmonics. Conversely, a 4 quadrant (4Q) converter has several advantages over the simple diode-bridges that make it a serious contender for our particular application.

In industrial power conversion it is well known that low voltage is most cost-efficient at low power levels while medium voltage is superior at high power levels. As the power ratings of wind turbines increase, medium voltage convertors become more competitive. Compared to low voltage convertors they employ fewer components, which is an inherent advantage with respect to reliability. We propose to use a General Electric MV7000 series convertor rated at 12MVA, 3.3kV, designed as a 4-quadrant water-cooled pulse width modulation (PWM) inverter. This convertor uses the latest generation of press-pack IGBTs with more power and lower losses making it an extremely reliable, efficient and high power density piece of equipment.

**Standards and Grid Codes - Fault Ride Through Requirements**

Based on the experience from the operation of power systems with large wind penetration levels, modification of the existing grid codes for connection and operation of wind power plants in the high-voltage grid have proven necessary. The objective of these provisions is to improve and stabilize wind turbine behavior, decrease the amounts of wind power to be lost following system disturbances and provide the wind power stations with operational characteristics similar to those of the conventional power plants. The most common requirements include fault ride through (FRT) capability, extended system voltage and frequency variation limits, active power regulation and frequency control, as well as reactive power/power factor and voltage regulation capabilities.

The occurrence of a fault (short-circuit) at some point of the network inevitably results in voltage dips in one or more phases (possibly also to a voltage rise in healthy phases), depending on the type and

location of the fault, which may be propagated to fairly remote locations of the network, especially in the case of weak grids.

The duration of the dips is dependent on the protection system response time and may vary between 0.1s and several seconds, the most usual duration being in the range of a few tenths of a second. In the event of such dips, generating stations may encounter stability problems, depending on the type, magnitude and duration of the dip, as well as on the type and technology of the power station. The large increase in the installed wind capacity in transmission systems necessitates that wind generation remains in operation in the event of network disturbances. For this reason, grid codes invariably demand that large wind farms (especially those connected to High Voltage (HV) grids) must withstand voltage dips down to a certain percentage of the nominal voltage (0% in some cases) and for a specified duration. Such requirements are known as FRT or low voltage ride through (LVRT) requirements and they are described by a voltage against time characteristic, denoting the minimum required immunity of the wind power station to dips of the system voltage. Certain codes impose increased reactive current generation by the wind turbines during the disturbance, in order to support the system voltage, in much the same way as a conventional synchronous generators increases its excitation during faults via Automatic Voltage Regulator (AVR) action.

Variable speed wind turbines, such as GE's superconducting generator, with full power converters present the distinct advantage that the converter totally decouples the generator from the grid. Hence, grid disturbances have no direct effect on the generator, whose current and torque variations during voltage dips are much lower compared with the doubly fed induction generator for example, and the respective transients fade out faster.

The converters, on the other hand, are almost (but not entirely) immune to grid transients, due to the high bandwidth of the PWM current controllers. The only essential issue that still remains is the imbalance between the generator power, injected to the dc side, and the output power to the grid, which may be drastically reduced, leading to overcharging of the dc bus capacitor. This can be resolved with fast pitch control and limited rotor over speed, to reduce the generator power, as well as via increased storage and possibly power dissipation means at the dc link.

From the point of view of the reactive output power, the grid side converter has the ability to produce reactive current during the voltage dip, up to its rated current capacity. It is noted that this wind turbine type may exhibit better voltage control capabilities than conventional synchronous generators. Hence, they can provide grid support (improvement of the voltage level and faster voltage recovery), with a positive impact on nearby connected stall wind turbines, reducing the probability of tripping for those turbines. Moreover, oversizing of the grid side converter provides enhanced active and reactive power in-feed capability.

## 1.1.3. Superconducting Coil Design

The superconducting coils used in the generator are racetrack coils wound with Cu-(Nb-Ti) low temperature superconductor. This section summarizes the design of the racetrack coils, the conductor used and the design optimization process used for these coils.

**Design Process**

The key design parameters for a racetrack coil are:

1) Coil width - which defines the number of layers in the coil
2) Coil height -which defines the number of turns per layer
3) Coil inner width (pole width) - which defines the inner width of the coil
4) End radius - defines the radius at the end of the racetrack coil
5) Coil straight length which is equal to the length of the generator armature core stack in this case
6) Position of coils, and
7) Radius of the cylindrical surface where the coils are located - i.e. the radius of the rotor or field coils.

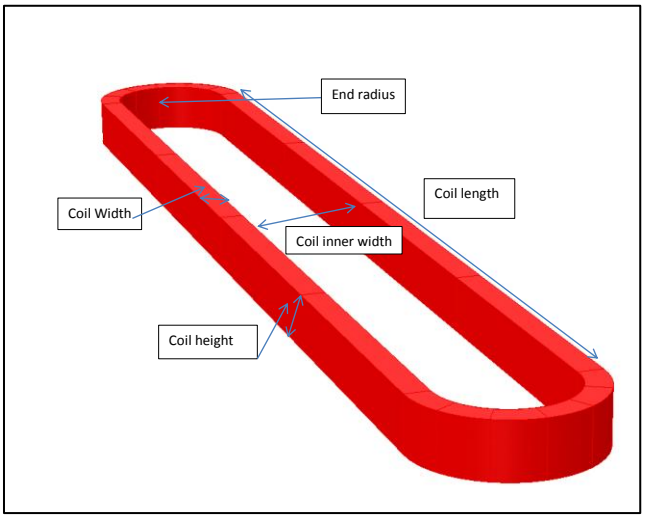


Figure 13 – Superconducting Racetrack Coil

Some of these parameters are governed by the generator design, namely the radius of the field coils and the straight length of the coil. For this optimization process the coil height is also kept fixed as it is an output from the generator electromagnetic design. A key parameter which is an input for the generator electromagnetic design is the magnetic flux density at the armature mid-slot position. The field at the armature mid-slot position provides a better representation of the flux linkage between the field coil and the armature than the field in the physical air-gap of the generator. The superconducting coils have therefore been optimized to produce the required field at this key position. The other parameters which are of significance for the safe operation of the generator are related to the superconductor being used. These parameters depend on the operating conditions of the superconducting coil, i.e. the operating current, maximum field in the coil and the current sharing temperature of the conductor.

**Superconductor selection**

The following conductor, from Supercon Inc. (Part No. SC-VSF-SSCI-1.0mm) has been selected for the SC coil based on availability, cost and performance.

Table 8 – Superconductor parameters

| Parameter | Value |
|---|---|
| Type of conductor used | Cu-(NbTi) |
| Cu:SC | 1.5 |
| Bare diameter of conductor (mm) | 1.00 |
| Insulated diameter of conductor (mm) | 1.05 |
| Number of filaments | 7400 |
| Filament diameter (micron) | 7.5 |
| Insulation | Formvar |

One of the key drivers in the selection of this high-filament number superconducting wire is to address the potential issue of alternating current (AC) losses within the wire under certain operating conditions which could lead to excessive heating and subsequent quench of the wire.

The important parameters for the conductor are the critical current at the operating fields and temperature; critical temperature $T_c$ at the operating temperature and field; and the current sharing temperature $T_{cs}$. At the current sharing temperature some of the superconductor goes normal and current sharing begins to occur between the superconducting filaments and the copper matrix. This can generate sufficient heat so that the entire conductor eventually quenches. The current sharing temperature is another measure of the safe operating margin for the coil. For the safe operation of a SC magnet, $T_{cs}$ is usually limited to a temperature 0.5 K higher than the normal operating temperature for bath cooled magnets and approximately 1.0 K higher for conduction cooled or cryogen free magnets. The cooling method for the SC coils in this generator lies between the two techniques as the coils are not in direct contact with liquid Helium, but there is liquid Helium used in the system. Therefore, the safe operating margin is assumed to be between these two values.

**Optimization of SC Coils**

The SC coil geometry was optimized for the following factors: End radius, Current in the coil, Coil block width and Coil inner width, with the objective (target) functions being:

1. Field at the air gap → Obtain required field at the armature mid-slot position
2. Current sharing temperature → Provide an adequate safe operating margin
3. Coil volume → Minimize the coil/conductor volume

The final optimized coil dimensions are shown later in Table 9.

The figures below illustrate the peak magnetic fields within the coils and provide an assessment of the available operating margin under the different operating conditions imposed by the generator. For clarity the field has only been plotted for one coil pair.

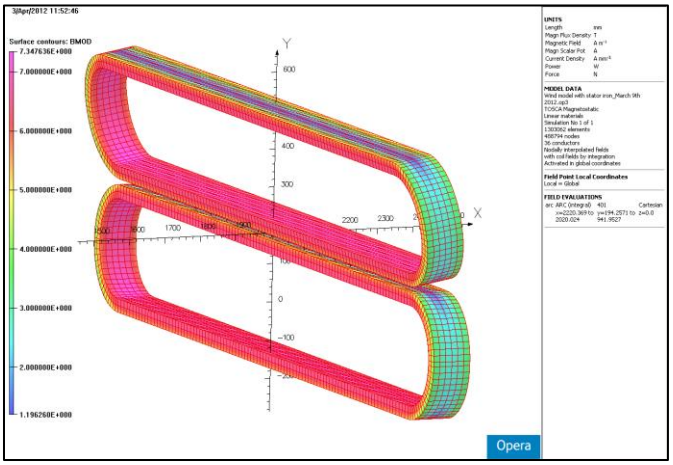


Figure 14 – Field profile in the coil indicating peak fields (Tesla)

The peak field in the coil approaches 7.32T at the innermost turns toward the ends of the coils.

The load line for the generator full load operating condition is provided below, indicating the operating current for a particular superconducting coil. The measured critical current of the conductor is plotted against the field. The point where the load line crosses the critical current line is the point where the

superconducting coil will go resistive. The operating current and the critical current at maximum field are shown below and indicate the available margin in operating current.

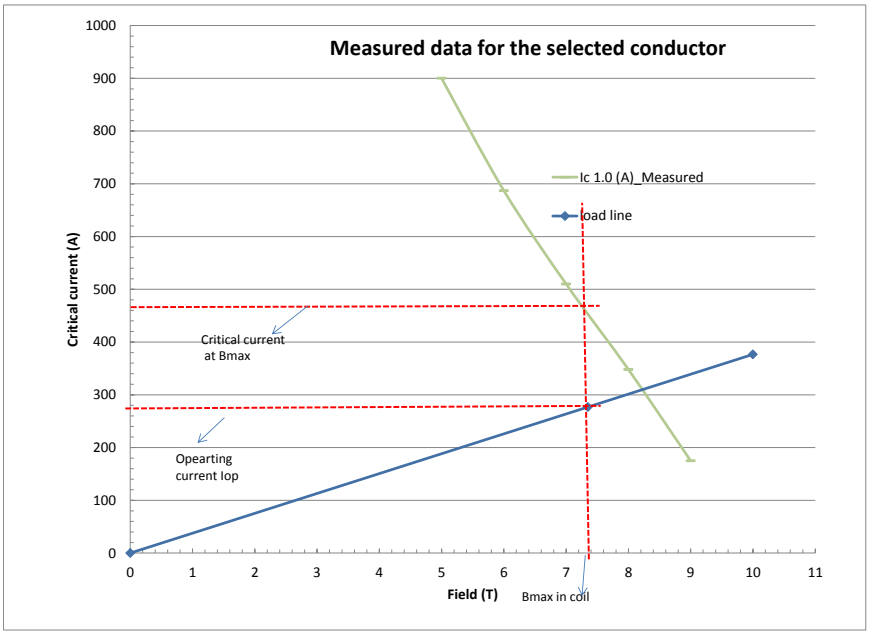


Figure 15 – Load line for the superconductor

Table 9 – Optimized superconductor field coils

| Parameter | Value |
|---|---|
| Coil type | Racetrack |
| Coil width (mm) | 35.00 |
| No. of layers in coil width | 39 |
| Coil height (mm) | 101.60 |
| No. of turns in coil height | 97 |
| Coil length straight (mm) | 1879.60 |
| Coil Inner Width (mm) | 261.01 |
| End radius (mm) | 124.58 |
| Type of conductor used | Cu-(NbTi) |
| Bare diameter of conductor (mm) | 1.00 |
| Insulated diameter of conductor (mm) | 1.05 |
| Operating current (Amp) | 276.86 |
| Total ampere turns (A) | 928000 |
| Maximum field in the coil (T) | 7.35 |
| Critical current at the maximum field (Amp) | 466.75 |
| Short sample percentage (%) | 59.96 |
| Critical temperature (K) | 6.08 |
| Stored energy of the system (MJ) | 40.6 |
| Inductance of all the coils (H) | 1059 |
| Total conductor used for 36coils (km) | 720 |
| Total estimated weight of the coils (kg) | 3840 |

The total superconductor required for the generator is still very high and is one of the largest cost drivers for this generator. The cost of the selected low temperature superconductor used for our machine is approximately 1/30$^{th}$ of the present cost of HTS conductor. The comparative cost of HTS conductor required for a 10MW (16 pole) generator would be approximately 5 times the conductor cost for LTS. Further coil optimization steps have been carried out and have been reported in Appendix D.

**Stray field**

From the point of health and safety of personnel carrying out maintenance activities on the generator (with the field winding energized), it is important to identify the extent of the stray magnetic field produced by the superconducting field winding. A secondary effect which may be important to quantify is the forces experienced by ferromagnetic objects within this stray field area – e.g. electromagnetically actuated parts on the cryocooler coldheads. The assessment (in terms of the location of the 5 and 500 Gauss field contours and field gradients) found no cause for concern both in terms of health and safety as well as effects on nearby ferromagnetic objects.

**A.C. Losses**

Although the SC coils are energized by direct current (DC), when these coils are ramped to the required operating current, losses are generated within the superconductor. Once the generator is in its normal operating condition, small variations in field and current could produce further losses and subsequently additional heat loads. These losses will ultimately determine the total heat load imposed on the cryogenic cooling system and will be related to the temperature rise in the SC coil during operation.

The AC loss calculations have been summarized below together with an independent assessment carried out by the Oak Ridge National Laboratory.

**1. Loss during normal operation**

A. Loss due to field current boost (this is required due to the inevitable droop in the field current due to the total circuit resistance; this is approximately 0.0584 A/s for our generator)

(a) Joint loss (D.C.) - i.e. due to joint resistances (operating current only)
(b) Intrinsic loss (D.C.) - i.e. due to index value, n (operating current only)
(c) Self field loss (A.C.) - i.e. boost current only

B. Loss due to external time varying fields (the different external fields will be (i) due to wind load variation, (ii) stator MMF harmonics, (iii) the slot/tooth passing frequency)

(d) Hysteresis loss
(e) Coupling loss
(f) Eddy current loss

C. Loss due to field current change (Field current change due to load transients=± 20 A)

(g) Eddy current loss

**2. Loss during ramping to operating field current**

(h) Eddy current loss
(i) Hysteresis loss
(j) Penetration loss

The following assumptions are made in calculating the AC losses:

- Operating current for the coils 276.86 A
- The total no. of coils is 36 and they are connected in series but in North-South configurations. There will be 3 joints per coil.
- The SC coils will be operated at 4.2 K.
- Calculated inductance of the whole SC coil system is approximately 1059 H. A ramp time of 8 hours is assumed for the initial energization of the field winding. However this is a variable that can be adjusted to allow for faster ramp times.
- Nb-Ti superconductor will be used for all the coils.
- Joint resistance is assumed to be $2.45 \times 10^{-8}$ Ω (worst case assumption).
- Resistance between coil and current lead is assumed to be $1.53 \times 10^{-7}$ Ω.
- Number of current leads= 2 (this number might increase after detailed quench protection analyses)
- Additional external circuit resistance = 0.5 Ω
- Ripple in the field winding DC current= 0.2% peak to peak @ 0.8 Hz
- Field current change due to load transients = ± 20 A
- Maximum field in the coil = 7.32 T

Total heat loads are as follows:

Total heat load for single sweep= 0.17 W
Total heat load during operation= 0.64 W

An Independent AC loss calculation has been performed by Dr. Robert Duckworth at the Oak Ridge National Laboratory (ORNL), based on the same assumptions provided above.

**Oak Ridge National Laboratory Assessment of AC Losses**

This estimate is based on the feedback that was received from Renuka Rajput-Ghoshal and Ruben Fair regarding the initial ac loss estimate and the practical implications for the assumptions that were made. In terms of tangible revisions that were implemented based on the discussion with GE Global Research:

1. *The average field in the coil winding is now assumed to be 4 T.*
    - Previous calculations were based on a peak dc field of 7.5 T, which was the maximum field generated by the coil windings. Based on modeling done by GE it is clear that across the cross section of the LTS coils the field varies between 2 T and 6 T on average. A value of 4 T was assumed for calculations but it should be understood that there will be some variation in the ac loss in the winding due to the variation of the critical current density and the fraction of the operating current to the critical current with respect to field.

2. *The contribution from the circuit resistances and joint resistances is neglected*
    - In the initial analysis it was assumed that both the circuit resistances **AND** joint resistances participated in the refrigeration heat load. This was a poor assumption as the circuit resistances were external to the coils and in the coils themselves. With the joint resistances expected to be well below 1μΩ, the heat load contribution at the operating current of 277 A is negligible.

3. *The ripple current in the coils due to the dc power source defined more clearly*
    - Based on the initial data provided by GE, it was assumed the ripple current had a frequency of 2-3 Hz with a current of 1%. Further investigation led to a revision of the ripple current based on the operating conditions with new values of 0.8 Hz and the percentage of 0.2%

***AC Loss Theoretical Formulations***

Based on these considerations and the revised projected performance of the coil during ramping and operation, an estimate for the ac loss in LTS coils was recalculated. Two expressions were used to estimate the ac loss in the LTS coils. The first is the hysteretic loss in the superconductor which for a superconducting filament assuming full penetration can be written (Wilson, Cryogenics 2008)

$$\frac{P}{V_{hys}}\left[\frac{W}{m^3}\right] = \dot{B}J_c\frac{2d}{3\pi}$$

with *d* representing the diameter of the superconducting filament (7.5 microns). The second is the dynamic resistance loss in the conductor due to the interaction of the dc current in the conductor to external and self-fields that are generated from the coils. This loss (Carr, AC Loss and Macroscopic Theory of Superconductors, 2011, p. 91) can be expressed

$$\frac{P}{V_{dyn}}\left[\frac{W}{m^3}\right] = \frac{4}{3\pi}\dot{B}J_c\frac{d}{2}g\left(\frac{I}{I_c}\right)$$

where g(*I*/*Ic*) is a function that is influenced by the fraction of the operating current to the local critical current, *I*/*Ic*. For the projected operating current of 277 A and a critical current of 750 A at the average operating field in the coil of 4.0 T, g(*I*/*Ic*) has a value of 1.1. In each of the models, a critical current density of 2290 A/mm$^2$ was assumed, which was based on the data provided for the critical current of the NbTi conductor at 4.0 T. It should be stated that often the formulas that are presented above have used the zero field value of the critical current density depending on the nature of the conductor. An increase to the critical current density would result in an increase to the estimates that are given below. Verification of the ac loss performance of the conductor and/or a prototype coil would provide some resolution as the appropriate assumption for the critical current density.

It should be emphasized that the formulas stated above are for the instances when there is full penetration of the applied ac fields in the conductor and the numbers that are presented represent a worst case scenario. Based on the assumed critical current density, the full penetration field value for the filament at 4 T is 27.5 mT. There may be many instances that the fields that are generated do not exceed this value, which would lower the observed losses given by the two formulas above. For the hysteretic ac loss, the ac loss would be written

$$\frac{P}{V_{hys}}\left[\frac{W}{m^3}\right] = \frac{(B_m)^2}{2\mu_o}\Gamma(\beta)$$

where $B_m$ is the magnitude of the field fluctuation, f is the frequency, and G(B) is a form function, which in the case of the assumed current operating current and dc field is approximately 0.4. With respect to the dynamic resistance, it is expected that this contribution would disappear as there has been observed a threshold effect in HTS materials and there is nothing in the literature on a dynamic resistance when the field is not fully penetrated into a round conductor. These assumptions on penetration would be things that could be investigated on a conductor basis and coil basis to determine their final impact on the coil design.

***AC loss from initial ramp of coils to operating conditions***

As the field is ramped from zero current to its operating current of 277 A over an 8 hour period, the rate of change in the field would be $2.6 \times 10^{-4}$ T/s. For the 1-mm diameter NbTi conductor with 7400 filaments with an average filament diameter of 7.5 microns, the hysteretic ac loss per unit length for the ***fully penetrated formulation*** was estimated to be $1.67 \times 10^{-7}$ W/m. This would translate to an ac loss per coil of 8.89 mW and an ac loss of 0.320 W for the entire 36 coil system as the system would ramp. This would not be an active refrigeration load, but ac loss would need to be accommodated as the coils are energized. A proportional increase in ramp rate would translate to a proportional increase in ac loss during the ramp.

***AC loss from current adjustment during steady state operation***

During operation of the coil, there are several different sources of loss that are generated from changes in the operating conditions as well as fluctuations from external fields and supply currents. The simplest one to account for is the change in operating currents on the order of +/- 20 A. If we assume that the rate for the change in operating current is on the order of ramp rate that is used to initially reach 277 A, which is 0.007 A/s, then the hysteretic ac loss contribution would be similar to value observed during the current ramp from zero current or 0.32 W. When compared to the hysteretic loss, it was found that the dynamic resistance ac loss contribution was comparable to the hysteretic with the ac loss per unit length per conductor of $1.74 \times 10^{-7}$ W/m. This would translate to an ac loss per coil of 4.12 mW and an ac loss of 0.352 W for the entire 36 coil system. As with the ac loss from the ramp rate, this ac loss would only be present during dynamic changes to the coil current and the frequency of this change in current would need to be analyzed with respect to the refrigeration cooling power to determine how often the current can be adjusted.

***AC loss from ripple currents during steady state operation***

The ripple current in the DC current is another possible source of ac loss in the system. If a 0.2% ripple current of 0.8 Hz on the 277 A dc supply current and ***full penetration*** of the filament is assumed, the hysteretic ac loss for the system was estimated to be 16.2W and the dynamic resistance ac loss for the system was estimated would be 17.8 W. Given that the ripple current is proportional to the loss, reduction of the ripple current would result in a reduction of ac loss.

Now there are a few issues to consider with the ripple current at the 0.2% level and 0.8 Hz. To operate the entire coil with a total inductance of 1059 H, the voltage across the coil would be 469 V. Limiting the voltage by either the control system or possible inclusion of a Shaft Voltage Suppressor (SVS) on the field winding (which is common practice for generating units), a reduction of the voltage across the coil down to 100 V would drop the hysteretic ac loss down to 8.15 W and the dynamic resistance ac loss down to 8.97 W. Another issue to consider is whether the ac loss is fully penetrated. For the ripple current that was specified, the fluctuation in field would be 13 mT. This value is below the 27.5 mT threshold for fully penetration, so the formulas used may be overestimating the ac loss. If it is assumed that this is the case and the third formula for partial penetration is used, the hysteretic ac loss would be 9.34 W without any changes to the coil operating voltage (608 V). If the same methods are used to reduce the voltage to 100 V, the hysteretic ac loss would drop to 0.452 W.

***AC loss from wind load variations during steady state operation***

The final contribution that was considered was the field fluctuations due to wind load variation as provided with Converteam data. Assuming a field fluctuation of 5 mT with a frequency of 1/40 Hz and full penetration of the filament, it was found the contribution from the hysteretic ac loss for the system was estimated to be 2.88 mW and the dynamic resistance ac loss for the system was estimated would be

3.16mW. This would be a fairly negligible amount, but as different contributions from the MMF harmonics and slot/tooth passing frequencies are accounted for this contribution would be evaluated.

It is not surprising to see these magnitudes of difference when attempting to model what is in fact a very complicated phenomenon, especially when the operating conditions for a wind turbine generator are markedly different from those of a static magnet system, such as a MRI machine.

It is therefore a strong recommendation that AC loss measurements be part of any further investigations. The results of these experiments will provide a path forward to either redesign the superconducting field coils to reduce these internal losses or to accommodate the losses with additional cooling. Depending on the outcome of the AC loss measurements the present conductor could potentially be replaced with a more standard conductor (i.e. - either with approximately 500 filaments or 54 filaments), which would reduce the overall cost of superconductor being used.

**Electromagnetic Shield Design**

An EM shield is normally required between the armature and the SC field coils to reduce the effect of varying fields and resultant losses within the field coils. A rotating magnetic field induces eddy currents within a conductor, which flow mainly within a 'thin' outer layer of the conductor called the 'skin depth'. The skin depth is a function of the frequency of the imposed varying field and is a measure of the depth at which the current density falls to 1/e of its value near the surface (***e*** being the base of the natural logarithm and is approximately equal to 2.71828). Over 98% of the current will flow within a layer 4 times the skin depth from the surface of a conductor. For an EM shield to be effective the shield thickness therefore needs to be approximately 4 times the skin depth. Skin depth (δ) is given by:

$$\delta = \sqrt[2]{\frac{2}{\omega\sigma\mu}}$$

where, ω =radial frequency (ω =2π f)
f = frequency (Hz)
μ =permeability of the material
σ =conductivity of the material (mho/m)

Skin depth calculations were carried out for the fundamental frequency of the generator (3 Hz) and 5 harmonic frequencies, these calculations were carried out for copper, aluminum and stainless steel.

For the fundamental frequency of 3 Hz, the skin depth for copper is approximately 38.15 mm, suggesting that for the shield to be truly effective, it should have a wall thickness of 152 mm which is far from practical. These components are physically further away from the armature and partially shielded have acceptable losses. Furthermore, the magnetic armature teeth have been shown to have a larger influence than the fundamental armature frequency on the eddy losses induced in the field components. The frequency of excitation due to the 36 teeth per pole pair is 36 times the 3 hertz fundamental, or 108 hertz. The skin depth for this frequency is much lower. For the frequency of 108 Hz, the skin depth for copper is approximately 6.36 mm and approximately 8.14 mm for aluminum, suggesting that for the shield to be truly effective, it should have a wall thickness of 25.4 mm of copper or 32.56 mm of Aluminum.

The field assembly consists of an aluminum alloy outer vacuum chamber (OVC) and an inner aluminum thermal shield. The wall thicknesses of these particular components have been sized based on mechanical considerations and ac losses due to armature coils on these components. The OVC thickness is 16mm and thermal shield thickness is 6 mm, this combination provides more than adequate shielding.

**Monitoring and Diagnostics**

An initial design of a Monitoring and Diagnostics system has been completed for the SC generator – primarily driven by the Failure Modes and Effects Analysis (FMEA) results. The temperatures on the superconducting field winding, armature winding, cold head and bearings will be monitored. Accelerometers will be used on the field coil and armature assemblies. The field coil voltage, current lead temperature, coil former temperature and field winding temperature will form part of the quench protection circuit. Quench back heaters may also be necessary as part of the quench protection circuit.

**Quench Protection Design**

The stored energy of the complete SC coil system is approximately 40.6 MJ. If this energy were to be dumped within the coils during a quench, the final temperature of the coils could exceed safe operating limits and could damage the coils irreversibly. The other possible scenario is that the coils are not damaged by high temperatures but that the temperatures reached would be too high thereby extending the cool down process for re-energization of the coils. A complete temperature monitoring, quench protection and energy management system will be required for the SC field winding.

The quench calculations are initially carried out only for two neighboring coils to obtain the current decay profile. A known heat source is introduced on the inner side of the coil to initiate a quench and the quench propagation is studied. The 2-coil quench analysis was carried out for two different scenarios (1) without coupling loss and (2) with coupling losses. These coupling losses are rate dependent i.e. a function of field change rate (db/dt) and as such are essential to model the effect of a quenching coil on its neighboring coils. The losses arise from two separate physical phenomena:

- Persistent currents in filaments: the power losses due to persistent current in filaments is given by ('Superconducting Magnets' by Martin Wilson)

$$P_f := \frac{2}{3\pi} J_c(B) d_f \lambda_{sup.} \frac{db}{dt}$$

Where, $P_f$ is power loss in Wm-3
$J_c(B)$ is the critical current at field B
$d_f$ is filament diameter
$\lambda_{sup}$ is fraction of superconductor in the wire
db/dt is the rate of field change

- Coupling current between filaments in the wire: the power losses due to coupling current between filaments in the wire is given by ('Superconducting Magnets' by Martin Wilson)

$$P_e := \lambda_{wire} \left( \frac{db}{dt} \right)^2 \left( \frac{1}{\rho_t} \right) \left( \frac{p}{2\pi} \right)^2$$

Where, $P_e$ is power loss in Wm-3
p is the twist pitch length
$\rho_t$ is effective electrical conductivity of the superconducting matrix at the operating temperature
$\lambda_{wire}$ is fraction of superconductor and copper in the wire

db/dt is the rate of field change

Superconducting coil temperatures during a quench event (with and without coil coupling being allowed for) are shown below.

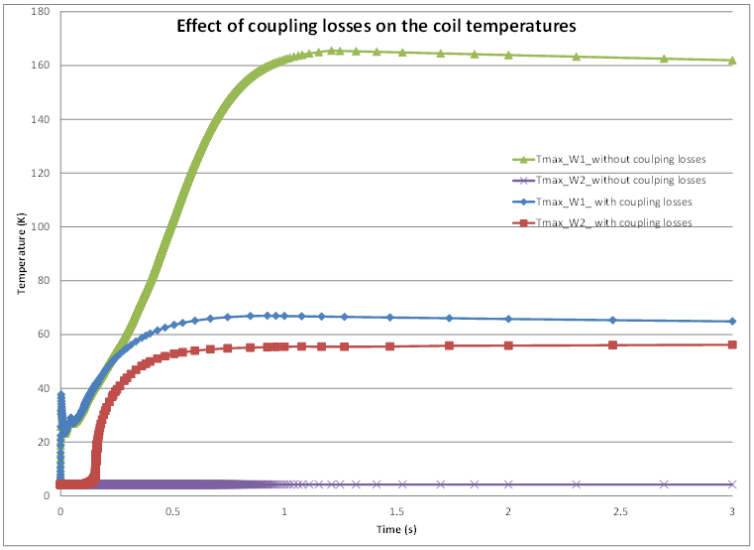


Figure 16 –Coil temperatures during a quench

It is clear from the above plot that coupling losses play a crucial role in the quench propagation process between coils. The peak temperature in the quenching coil reaches quite a high value (>160 K) while the other coil does not quench at all and its temperature stays at 4.2 K (the operating temperature) without the inclusion of coupling losses. After taking into account the coupling losses the 2$^{nd}$ coil now quenches and the temperatures in both the coils are fairly equally distributed. The peak temperature in the quench initiation coil is 65 K while it is approximately 55 K in the second coil. Note that the initial peak seen in the plot for the quench initiation coil is an artifact of applying heat to initiate the quench.

The important point to note is that rate dependent losses will naturally make neighboring coil quench and will distribute the stored energy in both coils which is a good thing.

## Field Winding Power Supply

The choice of power supply for the superconducting field winding will primarily depend on the tolerable AC losses experienced during ramping of the field current. It is also understood that any ripple in the output current of the DC power supply will increase the AC losses within the coils. Therefore selection of a suitable power supply with sufficiently low output ripple will be important.

The smallest commercially off-the-shelf (COTS) exciter that GE supplies would be the EX2100e typically used for small gas turbine generator systems and is rated for up to 600Vac input and 500A dc output which would be more than adequate for our needs. This exciter is a full-wave silicon controlled rectifier (SCR) bridge and can therefore force negative as well as positive voltages. This system consists of a control cabinet (600mm wide x 800 deep) and power convertor cabinet (1200mm wide x 800mm deep) and weighs 955 kg. It is a very complete system with all the required auxiliary functions including AC disconnect, AC line filter, field flashing from DC battery, DC contactor, de-excitation, redundant cooling fans and integral shaft voltage suppressor.

## 1.1.4. Cryogenic Cooling and Vacuum Design

A novel, low-cost cryogenic design concept for the 10 MW superconducting (SC) field coil assembly based on currently available technology, and more recent cross-over technology from GE's Healthcare business and GE-Global Research, has been analyzed. Care was taken to find solutions that were reliable, cost efficient and which allowed for fast and simple installation, commissioning and fault handling including cryocooler servicing.

**Design Process**

As a first step in this recursive design process, the dimensional parameters of the optimized field coils, including estimates of weights and forces, have to be known. Based on this information the cryogenic envelope is designed, and a selection of the cooling methodology is made. The next step is to optimize the cooling parameters including all operating conditions (cool down, steady state operation, events and fault scenarios) as well as the overall cost of the system and cost of ownership.

**Field Winding Assembly**

The field coil assembly consists of 36 individual race track coils each wound with conventional NbTi wire.

Figure 17 – (a) Aluminum 6061 coil former with machined race track coil pockets (36 pole design)

(b) Example of a typical single race track coil, showing lead in / lead out

After winding, the racetrack coils will be impregnated following a well-established vacuum pressure impregnation (VPI) process. The individual race track coils are embedded in a high-strength aluminum coil former (alloy 6061-T1). The low temperature superconducting coil assembly requires a good vacuum environment with the superconducting coils operating between 4.2 K to 4.9 K.

All structural and thermal components used in the field winding assembly are light weight either of aluminum (mass density 2700 kg/m$^3$) or titanium alloy (mass density 4540 kg/m$^3$).

### 1.1.4.1. Cooling concept

The superconducting coil with NbTi type composite superconductor will be kept cold at a constant temperature of 4.2 K using helium liquefying cryocoolers. For reasons of performance and cost of helium new technologies that enable a truly 4 K thermostatting cooling environment are introduced for the first time on this SC hybrid generator.

Since the field winding assembly is stationary in this hybrid SC generator design concept, rotating transfer couplings, forced gas flow with externally driven helium refrigerators to cope with the large heat loads are absent, and a novel cooling technology can be employed.

## Operating mode (steady state)

Due to the absence of any Helium vessel surrounding the field coils, the field winding assembly is now directly exposed to the thermal shield and other components allowing for a larger air gap to be utilized which has certain mechanical advantages.

Cooling loop tubes are placed in close contact to the coil former surface or even embedded in the coil former for good heat exchange. Space limitations imposed on the outer diameter of the field assembly due to air gap requirements required tube routing on the inner lateral surface. Figure 18 shows the implementation of the cooling loop tubes on the field coil former.

The cooling loop tubing consists of a well-sized liquid helium cooling ring at both flange ends and a linked structure on the inner lateral coil former surface. 4 cryocoolers will be used, 2 at each end, capable of liquefying gas bubbles and returning liquid to the coil former. The tubing is designed such that the cooling and liquefaction rate per cooler is uniform.

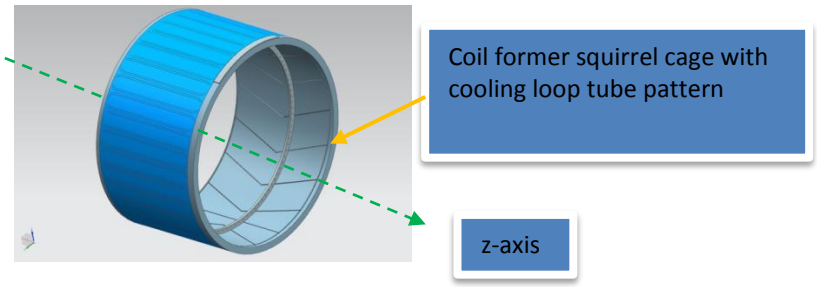


Figure 18 - Thin-walled stainless steel tubing fitted laterally at inner coil former

With all the tubing and reservoir filled with liquid Helium, gas bubbles move from the axial center of the field winding assembly magnet towards the outer toroidal reservoir tubes where they collapse on coming into contact with liquid. The volume taken up by the gas bubble is replenished by the liquid flowing down from the toroidal reservoir tubes. A small liquid Helium reservoir is fitted to the top of the non-hub end of the coil former. This top reservoir ensures that both toroidal tubes are always filled with liquid. This piggy back reservoir boils off liquid Helium due to the imposed heat load. The reservoir is connected to the cryocooler sleeve and its liquefaction cup at the bottom, collecting gaseous Helium from the reservoir and feeding liquid back to it as shown below.

## Cryocooler details


Figure 19 - Main components: cooler and MagMon (magnet monitoring system)

A Sumitomo RDK415 cooler is proposed and will be installed in a sleeve that is evacuated and enables coldhead (cooler) servicing but also partly protects the coldhead from a saline environment. The coldhead does not share the vacuum of the main cryostat.

We will be using 4 coolers for the field winding assembly cooling, 2 for the cryogenic infrastructure, 1 dedicated for cooling the torque tube and 1 as a backup cooler and for initial ramp to operating current.

All cryocoolers are located well below the 500 Gauss field lines, and will not be affected by the magnetic field of the SC field winding and will therefore not require any form of magnetic shielding.

## 1.1.4.2. Cryogenic Cooling (Thermal) Budget

All non-cryogenic SC generator design tasks will have repercussions on the cryogenic field winding assembly in terms of heat loads and must therefore be considered as a whole.

Based on this latest design iteration and taking into account stationary and transient conditions the heat losses are provided in the table below. As for the future, heat load reductions are possible with further progress in optimization steps.

Table 10 - Summary of steady state heat loads

| Component | Cryocooler 1st stage heat loads (W) | Cryocooler 2nd stage heat loads (W) | Source of heat load |
|---|---|---|---|
| OVC / TS Inner Wall | 20.38 | 0.8 | Radiation |
| OVC / TS Side Plate | 3.515 | 0.0625 | |
| OVC / TS Outer Wall | 29.869 | 0.807 | |
| Suspension struts | 1.235 | 0.0164 | Conduction |
| Residual gas | - | 0.06 | Conduction |
| Torque tube | 36 | 1.51 | Conduction |
| Coldhead sleeves / operation (4) | 15.5 | 0.563 | Conduction |
| Coldhead sleeve / cool down (2) | 1 | 0.2 | Conduction |
| Diagnostic wiring | 0.25 | 0.002 | Conduction |
| Current leads ( ) indicates ramp | 13.9 (25) | 0.2 | Conduction |
| Eddy current losses | 4 | 0.02 | Internally generated during operation |
| AC losses | - | 0.6 | |

## 1.1.4.3. Torque tube design and impact on cryogenic cooling

The torque tube is split into two parts, an “upper” and a “lower” torque tube to minimize heat leaks and to allow for ease of manufacturing. The lower torque tube develops a temperature profile from 300 to 40 K and the upper one from 30 K to 4 K. A detailed design effort has been carried out to reduce the cooling requirements of this vital structure.

The torque tube has to meet several design constraints:

- extreme torque load conditions with respect to buckling
- exceptional fatigue properties, and in particular at low temperatures
- light weight, ease of manufacture
- minimal heat burden to magnet coil former with respect to thermal conductivity
- minimal thermal radiation
- minimum of optically black cavities or so-called “black holes”
- simple and uncompromised application of MLI should be possible

Here several important conclusions of this analysis are given, based on thermal, mechanical and electromechanical calculations that all have repercussions on this design:

- To minimize heat loads a temperature below 40 K has to be maintained
- In the case of the abnormal 3-phase short circuit condition no additional heat load from the thermal shield must be transmitted to the coil former via the torque tube
- It is understood that the thermal shield should NOT warm up the warm end of the upper torque tube in case of an event

To comply with all above boundary conditions the warm end of the upper torque tube needs to be thermally insulated from the cold end of the lower torque tube and not heat-sunk to the thermal shield. The warm end of the upper torque tube is allowed to thermally float finding its own overall heat balanced temperature profile (< 40 K) and will be cooled via the heat path of the coil former only.

The upper torque tube, thermal shield and lower torque tube will have MLI applied to minimize thermal radiation heat loads. The chosen torque tube design considerably simplifies the application of MLI during the assembly stages.

Furthermore, the structural integrity is of utmost importance due to the huge torque loads. Because of fatigue reasons for this type of SC generator application, torque tube structures based on Carbon Fiber Composites (CFC) or Glass fiber Reinforced Plastic (GRP) cannot be used. Whereas the fatigue strength of TiAl6V4 substantially increases at low temperatures those values decrease for CFC or GRP as shown in Appendix C. TiAl6V4 has therefore been selected for the torque tube material for our generator.

**Normal Operating Conditions - Pre-cool process**

Offshore thermal mass cool down should be “touch of a button ready” without requiring handling of cryogenic liquids. In the following a novel design approach is presented using 2 standard Cryomech AL600 coolers to allow the superconducting field winding to be cooled down from ambient temperature to about 100K before the normal cryocoolers take over to reduce the temperature further to the operating point of 4.2K.

The figure below schematically shows the intended cryocooler attachment to the coil former. The vacuum vessel (OVC) is shown dotted, the coil former hatched. The coolers are fitted at the bottom of the field coil former. For the pre-cool, the cold head is pushed up against the object to be cooled (in the case the coil former). At the end of the pre-cool process, the cold head is retracted.

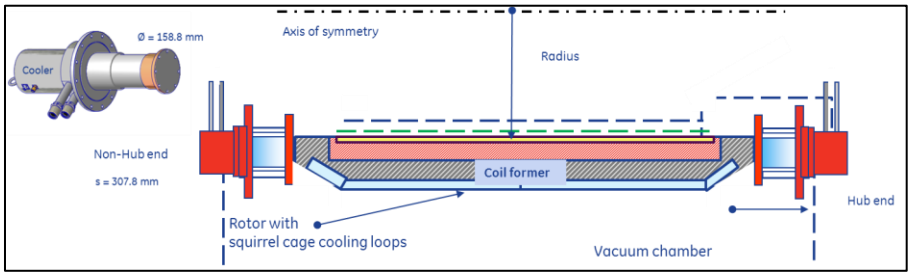


Figure 20 - Design intent – Cool down cryocoolers fitted to cold mass at hub and non-hub end

The actual cool down time strongly depends on the contact resistance between cooler and cold mass. The estimated cool down time is 7 ½ days.

**Abnormal operating condition - 3-phase short circuits**

In summary:

1. For a generator L-L-L short circuit from rated load, the field coil former will see a steady linear temperature rise until the field winding quenches. With the thermal protection circuit in place, this time slot should suffice to trigger an energy dump into the coil former in a controlled manner.
2. A generator short circuit would warm up the thermal shield only negligibly and the thermal shield would re-cool within 2 hours without imposing a big thermal radiation heat load on the coil former. The field winding assembly remains unaffected by this incident.
3. The air gap is cooled by cooling fans, the warmest layer of the superinsulation in the vacuum space will not directly see any heat spikes on the outer vacuum chamber.

## 1.1.4.4. Vacuum quality

In general the vacuum quality is compromised or deteriorated by the following:

1. Leaks into the vacuum jacket
2. Trapped volume in welds (and in bolt holes)
3. Incomplete pumping of superinsulation
4. Degassing of superinsulation
5. Degassing of plastic structural supports
6. Degassing from vessel walls
7. Incomplete removal of helium introduced during leak detection
8. Hydrogen diffusion process in metals

For superconducting systems with a thermal shield with an operating point of 40 to 45 K and a cold mass remaining at 4 K, only Item 8 is of interest since all other items are either taken care of by the correct work and assembly instructions or by allowing degassing to occur and condense at cold surfaces (cryopumping).

It should be stressed that no specific means need to be employed to maintain good vacuum other than good work practice, for example, cleaning metal parts after machining to remove oil, or storing the superinsulation in a dry place prior to assembly.

Other than that no other means need to be implemented. There is no special material treatment required (bake out) to accelerate outgassing/degassing of surfaces. Being able to maintain excellent vacuum quality is one of the big advantages of operating at 4 K, reduces cost immensely and allows for a safer performance as compared to SC generators operating at 20 K and higher.

## 1.1.5. Mechanical Design

There are four major areas of work on mechanical design for this superconducting generator design. These include the generator supporting structure, the field winding assembly structure design, the bearing design and the brake design. The generator support, the bearing and the brake design provide mechanical architecture to:

1) support generator rotating armature and stationary field interaction under both wind and electromagnetic extreme load
2) to connect generator with wind turbine shaft, upstream hub and downstream supporting structure under extreme load
3) to provide proper function for the wind turbine generator.

The field winding assembly design is unique to superconducting generators of this type due to the cryogenic environment and extreme load associated with the application. The challenges lie in that the design has to meet both mechanical integrity and temperature requirements.

**Loading conditions**

In order to properly size the mechanical components, estimates were made to quantify the extreme wind loads. Typically the tool used to make these calculations for detailed design efforts is FLEX5. Certification organizations have accepted the FLEX5 results as accurate. FLEX5 models the environmental conditions, the aerodynamic and elastic response of the turbine components, and the control of the turbine to determine the loads and deflections at any moment in time. A modal approach combined with time stepping is used.

For conceptual design efforts consistent with this project, instead of using FLEX5 and its corresponding long execution times and high amount of data generation, an internally developed tool exists for estimating the extreme loads. This tool uses a design-of-experiment of loads created using FLEX5 and interpolates the estimated nominal and extreme loadings based on a number of variables. This tool has been validated internally and for this project the results were reviewed with the loads team to ensure the values were sufficiently accurate. The magnitude of both the nominal and extreme hub moment loads can be found in Table 11. These resultant moment loads are applied in the nodding direction as a worst case condition and the other wind related forces were neglected due to their fairly insignificant role in the conceptual design process.

In addition to the wind loads, the electro-magnetic forces also have a significant influence on the mechanical design. There is a nominal attractive force between the concentric field and armature, an additional force due to a change in the relative distance between the field and the armature and an extreme torque created by an electrical fault in the generator. The extreme torque value used in the mechanical design assumes a fuse or circuit breaker type mechanism will be used to limit the observed torque to approximately three times the nominal torque value.

Table 11: Loading conditions for the mechanical design

| | Nominal | Extreme |
|---|---|---|
| Hub Moment | 5.8e9 N-mm | 5.1e10 N-mm |
| EM Radial load | 160 psi | 160 psi + 5.5e6 N/in*air gap delta closedown |
| EM Torque | 9.554e9 N-mm | 2.7e10 N-mm |

**Design Process**

Several different structural layouts were considered but ultimately an overhung two bearing system with conical support structures was selected due to its simplicity and structural efficiency. The most limiting load case for both stress and closedown occurred when applying the extreme wind moment load along with the electro-magnetic attractive forces. An iterative analysis process was required to properly assess the full effect of the combination of these loads. The structural design specifics such as diameters, thicknesses, lengths and angles were iterated on to ensure the closedown and stress limits were met in the final design.

The expertise and established design practices of the wind division of GE was leveraged to drive the initial shaft sizing and bearing selection. The transmission analysis software MASTA was used to estimate the translational and rotational stiffness of the custom bearings. These stiffness values were incorporated into the system level finite element model for proper estimates of the relative closedown of the air gap between the armature and field. As the overall structural design evolved, a second iteration was made on the bearing size and stiffness to ensure an accurate and complete bearing assessment. These latest bearing designs were incorporated into the final structural analysis. Additionally, an initial parking brake sizing calculation was done to estimate the requirements for a typical caliper and disc system.

The field assembly for this type of a generator poses a very unique challenge. This assembly needs to handle fairly significant structural loads with the least amount of material possible in order to minimize the cryogenic cooling requirements. To meet this challenge, a detailed field sub-assembly structural model was created. Under the extreme EM loads, the initial analysis suggested the torque tube would buckle when subjected to just a fraction of the extreme loads. Simple approaches to resolve this buckling issue were not feasible given the tight cryogenic cooling requirements. Therefore, a unique torque tube design was developed and incorporated. Analysis shows this new design provides the necessary stiffness to avoid buckling while minimally impacting the cooling requirements of the system.

## 1.1.5.1 Armature and Field Support Systems

A two bearing layout was selected due to its simplicity and minimal weight potential. While the use of overhung structures is a little unique, the general concept of a two bearing layout is similar to others currently used in the wind industry and poses no significant additional risks to the overall system.

Traditionally any wind turbine larger than a 1.5MW is fatigue limited by the main shaft which transfers the wind loading from the hub to the main bearings and ultimately to ground. Therefore, the dimensional requirements of the main shaft dictate the bore of the main bearings. The stationary shaft outer diameter was determined by accounting for the wind extreme and fatigue loads. A suitable cast material, was chosen to provide a cost effective way to manufacture this shaft design.

Once the main shaft was configured to handle the loads based on wind design practices, it was then possible to design the bearings to establish bearing sizes and stiffnesses.

The expertise and established design practices of the wind division of GE was leveraged to drive the bearing layout and calculations. A double row tapered roller bearing was selected to support radial, axial, and bending loads, and when used with a floating cylindrical bearing, has high field reliability. Figure 21 shows the selected bearing layout. With this design, the axial loads are efficiently transferred from the hub flange through the tapered bearing and into the stationary shaft and out to ground. Both these bearings are greased and do not require any auxiliary cooling or oil systems. They will require lubrication every 6 months to 1 year which is typical for main bearings of existing wind turbines. The bearings were designed for a load capacity that would allow them to have a lifetime of 20 years.

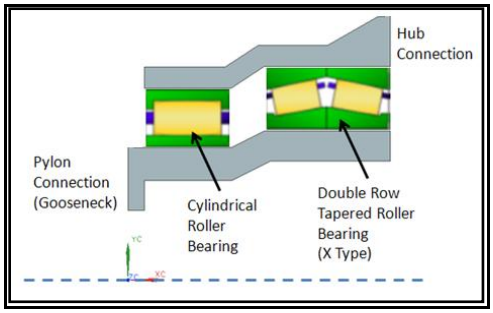


Figure 21 – Bearing types and layout

With the bearing type, configuration, and internal geometry designed, it was possible to calculate the bearing stiffness. These three components are the main drivers for bearing stiffness, and since it is an iterative process, MASTA transmission analysis software was used to calculate the bearing stiffness in the radial, axial, and tilt directions.

One unique aspect of this structure relative to typical wind turbine generators is that the axial length of the shafts is short relative to their diameters. This effect results in peak stresses driven primarily by transverse shear rather than bending. To alleviate these high stresses and also reduce the vertical deflections, a shaft sensitivity and optimization analysis was performed.

The next focus was determining a reasonably stiff way to connect these shafts to their respective generator components. Given the cantilevered design, this support is critical for controlling the gap between the armature and field assemblies. Two concepts were explored with the conic support structure finally being selected as the most suitable for our application.

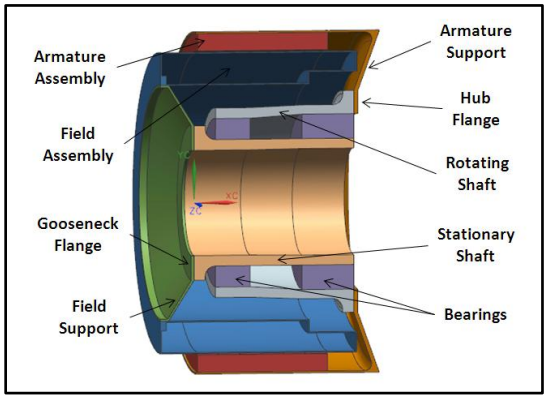


Figure 22 – Updated Conic Support Structure Layout

To quantify the deflections and stresses of the final design, a series of finite element analyses were performed. The first was an assessment of both the field and armature supports under the extreme torque load. For this analysis, a full 360 degree model of only the two supports was used. Figure 23 shows the geometry, applied boundary conditions and resulting stresses.

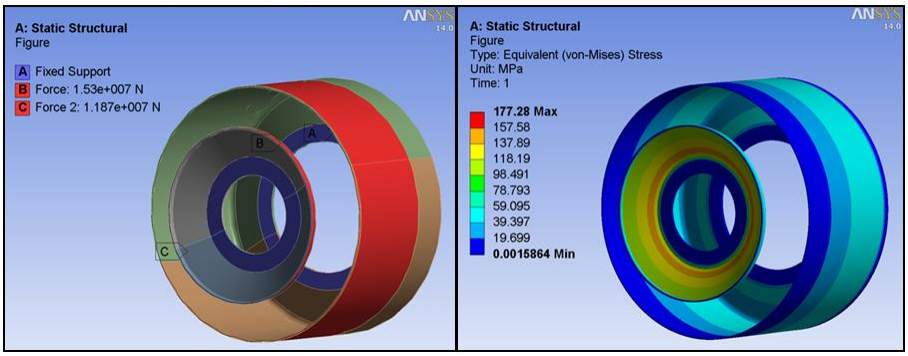


Figure 23 – Support Torque Boundary Conditions and Results

As expected, the highest stresses occur near the ID of the supports. Since the field support is both thinner and has a smaller ID, it has higher stresses than the armature support. The maximum equivalent stress in the field support is ~177 MPa. This represents a safety factor of ~ 2.1 since the ductile iron material has a yield of 380MPa. The armature support is clearly well within these stress values and can easily handle these extreme torque values.

Since the attractive force between the field and the armature changes as a function of their proximity, the method for analyzing the final air gap closedown must be iterative. Table 12 summarizes the air gap close down figures together with their associated safety factors for the 4 load conditions.

Table 12 – Air Gap Closedown and Max Stress Values

| Load Case | Air Gap Closedown | Max Equiv. Stress |
|---|---|---|
| 1 – Gravity Only | 0.9 mm (5%) | 20 MPa (19.0 SF) |
| 2 – Gravity, Nom. Wind | 1.7 mm (9%) | 35 MPa (10.9 SF) |
| 3 – Gravity, Nom. Wind, EM | 2.3 mm (12%) | 37 MPa (10.3 SF) |
| 4 – Gravity, Extreme Wind, EM | 7.8 mm (41%) | 287 MPa (1.3 SF) |

Finally, the weight of each of the key generator components was estimated from the model. The sum total of all the components listed is approximately 139 metric tons. While some effort was made to avoid having unnecessary mass in the system, there is still an opportunity to further reduce the weight with a more detailed optimization effort. Recent studies at GE-GR have demonstrated the ability to reduce the weight of major structural components by an average of 10-20% through the use of various topology and shape optimization design tools. This approach could be applied to the support and shaft components, with the potential to reduce the overall weight of the system to around 111 metric tons.

## Mechanical Brake

As is typical for wind turbines, the brake incorporated into the design is intended to be used as a parking brake. The brake system consists of hydraulically actuated calipers with brake pads, a disc attached to the rotating armature and a shear pin engaging mechanism. Before engaging the brake calipers, the turbine blades would be aerodynamically feathered to remove the input load to the system and the system would be allowed to slow down. The brake would then be used to hold the disc and prevent the armature and hub from rotating. This brake system also allows for a shear locking pin to be inserted into the disc as a safety precaution or in the case of a prolonged downtime. For sizing purposes, it is assumed that even though the blades have been feathered there still exists the possibility that a gust of wind could switch direction and effectively generate a load consistent with full power. This 10MW potential results in a minimum disc diameter of 3700mm and between 4 and 8 calipers.

## 1.1.5.2 Field Winding Assembly

Figure 26 shows the preliminary design of the superconducting field winding assembly. The innermost component of the field assembly mechanical structure is the coil former which supports the superconducting field coils operating at 4 Kelvin. The coils are held within individual pockets on the former by aluminum closure plates which are bolted to the main body of the former. The magnetic field generated by the field coils interacts with the iron armature and the armature windings producing forces which are seen by the field coils and the field coil former itself. A torque tube is used to connect the coil former (at 4 Kelvin) to the outer vacuum chamber (OVC) wall at 300 Kelvin. The torque tube has two purposes – to transfer torque and radial loads from the field coils to the field assembly support structure and to provide a thermal break between cryogenically cold parts and parts at ambient temperature. The torque tube consists of an upper portion connecting the coil former to an intermediate thermal shield (TS) via bolted flanges; and a lower portion connecting the thermal shield to the outer vacuum chamber – again via bolted flanges. The torque tube is designed not only to be stiff enough to support the complete coil assembly, but also long enough to sustain the thermal gradient from 40k at the TS to 4k at the coil former, and from 300k at the OVC to 40k at the TS. The thermal shield is an intermediate thermal radiation shield cooled to about 40K. The OVC encloses the complete set of superconducting field coils and is evacuated to a very low pressure (usually of the order of 1 x $10^{-5}$ mbar or lower) to reduce heat loads onto the cryogenically cold components housed within the OVC. Multi-layer insulation blankets are wrapped round the thermal shield providing further thermal radiation shielding.

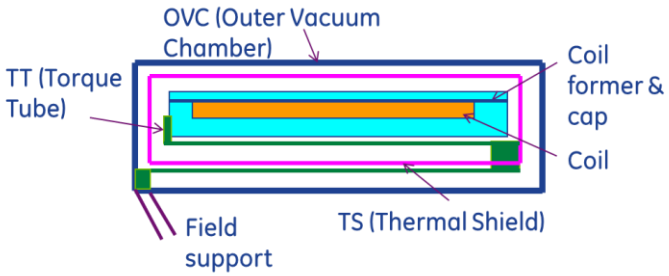


Figure 24 - Preliminary design of the field assembly

**Design Process**

Analysis was performed to understand the behavior of the field assembly under extreme electromagnetic (EM) loading conditions as well as gravity. Initial static and buckling analyses indicated that the preliminary design of torque tube would buckle at only 8% of the extreme load, long before the structure reached its stress limit. This occurred because the torque tube is constructed from thin walled cylinders which do not have the required stiffness to transfer the imposed loads. Increasing the wall thickness of the torque tube elements as well as shortening the elements would have increased the stiffness values – however this would also have increased the conduction heat loads onto the cryogenically cold components. The torque tube design process is therefore iterative and has to satisfy both the stiffness and thermal loading requirements.

Two solutions are proposed to qualify the field assembly design – firstly by leveraging the geometry of the torque tube to overcome buckling and to meet the cooling requirements; secondly to utilize thermal barriers between the torque tube flange and the thermal shield to reduce the conduction heat load.

**Torque Tube (TT) Design**

Increasing the toque tube wall thickness, reducing its length, and adding patterned features onto the face of the material can all serve to increase the stiffness of this key component.

A technique called Structure Optimization Technology was used to find the optimum stiffening pattern for the torque tube. A Design of Experiments (DOE) study was performed to optimize this stiffening pattern. The design variables for both the upper and lower elements of the torque tube are shown in the table below. The final design values enable the torque tube to meet both the buckling requirements and the cooling budget.

Table 13 - DOE design variable specifications

| | **Design variable** | **Baseline (mm)** | **Range** |
|---|---|---|---|
| Upper TT | Thickness | 4 | <6.5 mm |
| | Axial length | 2585 | <2585 |
| | Number of stiffening feature | N/A | N/A |
| | Contour length | N/A | The longer the better |
| Lower TT | Thickness | 5 | <10 mm |
| | Axial length | 2720 | <2720 |
| | Number of stiffening feature | N/A | N/A |
| | Contour length | N/A | The longer the better |

The next step in the design process was to model the complete field assembly to understand its behavior when subjected to the extreme loads described earlier.

Both static and linear analyses under extreme load were performed to prove the conceptual design of the field winding assembly. The analyses show that the new design will pass the buckling requirements with a buckling factor of 1.5, even for the extreme load condition. This means that the assembly can take ~4.5x EM nominal torque before it buckles and the safety factors shown below confirm this.

Table 14 - Field assembly static analysis results under extreme EM load and gravity

| | Material | Working temperature (K) | Tensile Strength, Yield (Mpa)* | Max Stress (MPa) | Max Stress SF | Max Radial displacement (mm) | Max Rotational displacement (mm) |
|---|---|---|---|---|---|---|---|
| OVC | 6061-T6 | 40-300 | 288 | 30 | 9.6 | 0.03 | 0.04 |
| TS | 1100 | 40-60 | 63 | 10 | 6.3 | 1.22 | 15.25 |
| Upper TT | TiAl6V4 | 4-40 | 1132 | 390 | 2.9 | 1.63 | 20.98 |
| Lower TT | TiAl6V4 | 40-300 | 1926 | 338 | 5.7 | 0.94 | 14.01 |
| Coil former | A356-T61 | 4 | 330 | 78 | 4.2 | 2.54 | 23.70 |
| Coils | NbTi composite | 4 | 190 | 34 | 5.6 | 2.51 | 23.60 |

**material properties at working temperatures*

The improved field assembly, and in particular the torque tube was put through the cooling power calculation to reconfirm that the heat loads did not exceed the cooling budget. Table 15 compares the cooling power required and cooling budget allocated for the torque tubes. The lower TT meets the cooling requirement while the upper TT requires higher cooling power than allocated. Our study in the next section shows that the use of a suitable thermal barrier can help reduce the heat load impact on the torque tube.

Table 15 – Cryogenic cooling requirements for torque tube design

| | Cooling power required | Cooling budget allocated (W) |
|---|---|---|
| Upper TT | 2.6 | 2 |
| Lower TT | 36 | 40 |

## Thermal barrier design

Cryogenic cooling requires any connecting components to be as long and as thin as possible to limit conduction heat losses. However, structural loads necessitate thicker structures to handle stresses, and deflections such as buckling.

The required temperature for the coil former is 4K. It is a requirement that the upper torque tube temperature should not exceed 50K. The thermal shield should also be around this temperature. These requirements can be met by placing a thermal barrier between the torque tube flanges with the TS sandwiched in between.

A preliminary thermal analysis for conduction and radiation heat loads was performed for the field assembly indicating that the maximum temperature at the joint inside the thermal shield is 46K. Further optimization will be carried out to further reduce the thickness of the thermal barriers without sacrificing mechanical rigidity.

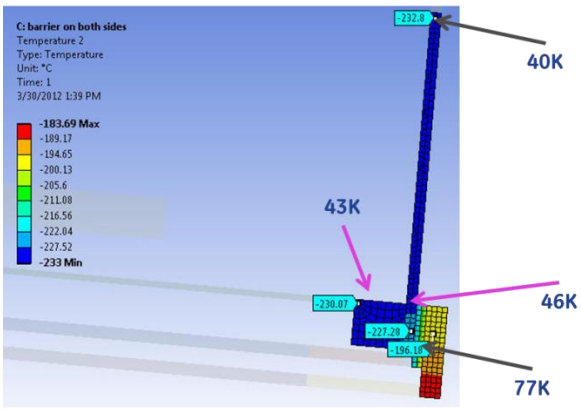


Figure 25 - Thermal barrier thermal steady state results

## Bolted joint design

A clear understanding of the boundary conditions of the field assembly is necessary to develop a feasible and cost-effective design while operating within the following constraints:

- The assembly is subjected to extreme temperature ranges. 300K at the OVC to 4K at the former
- Components are constructed of different materials with different coefficients of thermal expansion.
- The coil former is subjected to large tangential, radial, and eccentric fluctuating loads
- Heat conduction at key locations of the assembly needs to be minimized

With the listed constraints we could consider at least three choices

1. Press fit or shrink fit of the different components
2. Bolted joints
3. Match machined bolts or dowel pins

A press fit was not considered because it would require very precise tolerances (which can be very difficult to maintain for such large parts ~ 4m diameter) and large interference values due large loads. The next option was to require the bolt shank to take the shear/tangential load due to EM torque. The scenario would require the bolts to be match machined. We selected M24 bolts, class 8.8.

Table 16 - Bolt joint calculation

| | | |
|---|---|---|
| Bolt dia | 24 | Mm |
| Bolt area | .00045239 | m^2 |
| # of bolts | 100 | |
| Load | 1.366E7 | N |
| Shear stress load | 3E8 | Pa |
| Bolt yield for a M24 | 6.6E8 | Pa |
| Bolt yield shear (.6 of yield) | 3.96E8 | Pa |
| Safety factor | 1.3 | |
| Bolt circle circumference | 13.3 | m |
| Arc per bolt | .13 | m |
| Arc per bolt | 133 | mm |

This possible solution would require 100 M24 bolts, with 133 mm spacing between bolts. Each torque tube flange would need to be at least 48 mm thick.

The next step would be to consider bolts made of different materials such as Inconel to reduce their thermal effect on the electrical machine. A more detailed bolt analysis and testing will also need to be performed.

# 1.2 SOPO Task Number 1.2 - Evaluation of the designs for their economic, environmental and commercial consequences

## 1.2.1 Technology Readiness Level Analysis

A Technology Readiness Level (TRL) analysis has been completed for major subsystems. The criteria used for the analysis is described in Appendix C on a scale of 1 to 9.

The main thrust of this project has been to utilize, wherever possible, either conventional technology and established production processes or to ensure that the transference of technology from one application area (e.g. Healthcare) to another area (Wind) is accomplished using best practice. Figure 26 summarizes the findings. The TRLs have been determined for Phase 1 and also for Phase 2 – i.e. before and after the risk mitigation work has been completed.

Further analysis of the data displayed in Figure 26 below indicates that the TRLs can be segregated into 4 broad sub-system categories: Armature, Superconducting Field, Cryogenic Cooling and Mechanical. Table 17 summarizes the percentage of key components within each sub-system that fall below TRL 4 as identified during Phase 1 and the potential improvement at the conclusion of Phase 2.

Table 17 – Percentage of key components lower than TRL4

| | PHASE 1 | PHASE 2 projected |
|---|---|---|
| **Sub-System** | **% lower than TRL4** | **% lower than TRL4** |
| Armature | 10 % | 0 % |
| Superconducting Field | 28 % | 0 % |
| Cryogenic Cooling | 0 % | 0 % |
| Mechanical | 43% | 28 % |

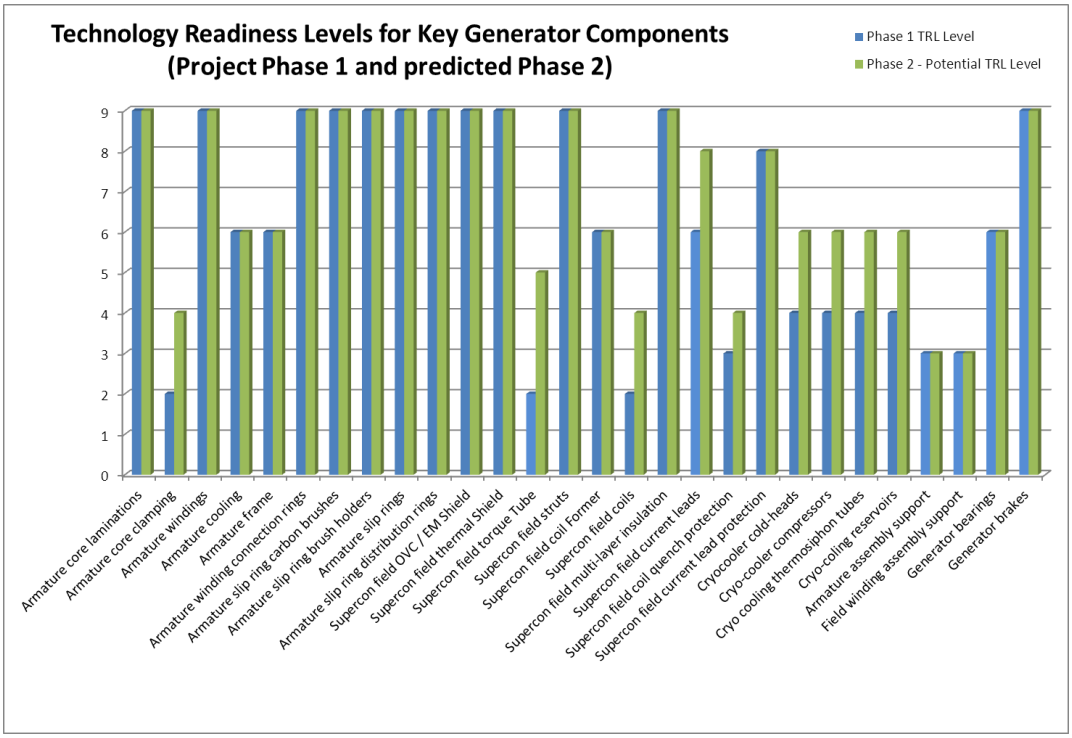


Figure 26 – Technology Readiness Levels for Key Generator Components

Several key points to note:

a) Although several items identified in Figure 26 may be related to the superconducting field coils, they are in fact part of the mechanical sub-system (e.g. Supercon field struts, Supercon coil former, Supercon field torque tube). Similarly, there will be other components, e.g. armature core clamping, which is related to the mechanical sub-system but in reality affect the cooling or electromagnetic performance of the machine and will therefore be treated as part of that sub-system.

b) It will be noted that not all the key mechanical components will be able to be addressed within a laboratory environment (e.g. the armature and field winding assembly support structures – these refer to the large conical structures that connect the armature and field winding assemblies to the generator shafts. Further detailed mechanical analysis will need to be performed on these structures, but prototype build and demonstration of these structures may not be possible)

## 1.2.2 COE Analysis

### 1.2.2.1 Updated Impact on Reducing COE

The proposed 10 MW low-temperature superconducting (LTS) direct drive generator wind turbine has the potential to reduce the cost-of-energy (COE) by 13% as compared to the permanent-magnet direct drive (PMDD) 5 MW baseline turbine. The baseline PMDD generator cost and performance is optimistic compared to the present state-of-the-art specifically with the recent rise in price of rare-earth metals which are required in these generators. If one compares to, for example, a 5MW geared drivetrain, the approximate COE reduction would be even larger, estimated at 18%. Table 18 summarizes the operating parameters for the two baseline turbines and wind plants as well as the proposed LTSCG configuration. The calculated COE impact follows a consistent methodology as specified in the Request for Proposal (RFP) and the detailed COE calculation tables can be viewed in Appendix D. Appendix D also includes detailed calculations for scaled-up versions of PMDD and geared turbines at the same configuration as the proposed LTS generator.

Table 18 – Summary of Turbine & Wind Plant Operating Parameters

| Description | Baseline PMDD Comparison | Baseline Geared Comparison | Proposed LTS Gen Configuration |
|---|---|---|---|
| Wind Plant Rating (MW) | 250 | 250 | 250 |
| Turbine Rating (MW) | 5 | 5 | 10 |
| Rotor Diameter (m) | 126 | 126 | 160 |
| Hub Height (m) | 95 | 95 | 112.0 |
| Distance to Shore (km) | 25 | 25 | 25 |
| Water Depth (m) | 30 | 30 | 30 |
| Wind Speed @ Hub Height (m/s) | 10.0 | 10.0 | 10.2 |
| Max Rotor Cp | 0.482 | 0.482 | 0.482 |
| Specific Power (kW/m2) | 0.4 | 0.4 | 0.5 |

Figure 27 depicts the major COE categories summed to an overall COE.

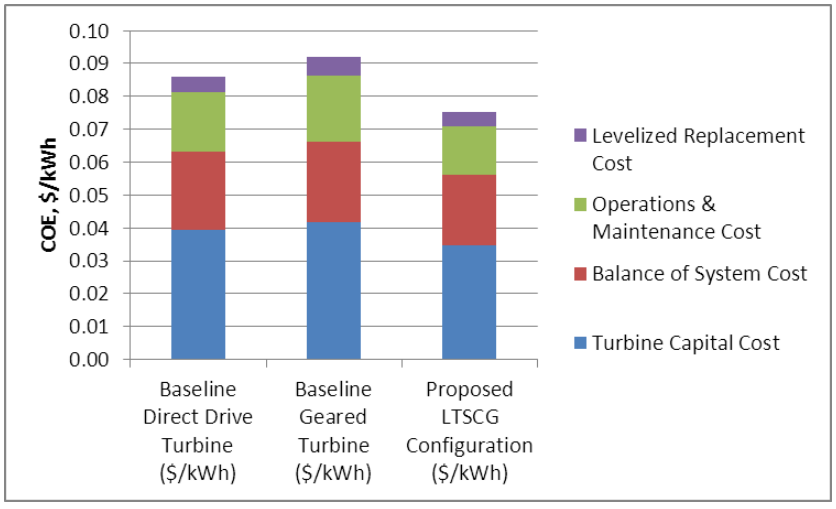


Figure 27 – Comparison of Wind Energy Systems COE

The fundamental COE reduction for the proposed concept is through an increase in generator torque density which substantially decreases the mass and cost of the generator. This large reduction in generator cost allows the turbine to scale to 10MW while still maintaining a reduced turbine specific cost ($/kW) as compared to the baseline. The turbine's optimal specific power ($kW/m^2$) also increases from the baseline of $0.4kW/m^2$ to $0.5kW/m^2$ since the sensitivity of the turbine cost to the rating is decreased through the lower cost generator. Increasing the turbine rating provides an economies-of-scale advantage in the Balance-of-System (BOS) costs, since there are fewer turbines and reduced length of collection cables to install to achieve a given power output. Finally, the increased turbine rating also reduces operation and maintenance (O&M) and levelized replacement costs (LRC) through similar economies-of-scale. With fewer turbines to service, the servicing cost drops since a portion of those costs are the labor and use of vessels to access the turbines. Also, since the turbine cost is less expensive in a $/kW basis, the cost of replacement components would be less expensive resulting in even lower O&M and LRC costs.

The mass and cost for the proposed superconducting wind turbine direct drive generator was estimated by updating a bill of materials (BOM) for the concept based on the results of Phase 1 of the project. From the BOM, cost estimates were collected using actual quotes from a variety of sources including the GE businesses and selected vendors. Assumptions were necessarily made with regards to where and how the generator was going to be manufactured. As far as possible, standard manufacturing techniques will be utilized for the armature and current collector system while stationary field winding and associated cryogenics and vacuum technologies will draw upon methods already in place within the GE Healthcare business. GE's robust quality control process will be applied to all aspects of manufacture and test of the final machine. The top ten component cost portions of the LTS generator are summarized in Table 19 below which includes the costs of the bearings and armature and field shafts. The cost of the proposed generator is dominated by the superconducting wire and therefore, future design work should concentrate on minimizing the amount of wire needed. In fact there is a possibility of reducing the number of field poles (and hence superconductor wire) but at a cost to overall machine weight – this has been discussed later in Section 1.2.3.

Table 19 – Summary of generator component costs

| Component | Cost (%) |
|---|---|
| SC wire | 33 |
| Torque tube | 11 |
| Two bearing unit | 11 |
| Coils with insulation | 6 |
| Cool down cooler | 4 |
| Cryocoolers | 4 |
| Armature shaft | 4 |
| Quench protection | 3 |
| Field shaft | 3 |
| Core end plates | 3 |
| Other | 18 |

Figure 28 shows the 30 to 39% reduction in drivetrain cost that the proposed LTS generator configuration provides. This reduction is a conservative estimate and could be much higher if the PMDD generator cost incorporated the recent price increases of rare-earth metals and if cheaper superconducting wire was sourced. Also included in this plot is the drivetrain cost of a high temperature superconducting (HTS) generator provided in Maples et al [1]. Although this example HTS configuration at 10MW is not

consistent with the 10MW design in this study (the current study has higher torque), it does provide an example of the overall cost and demonstrates a 28% reduction in cost with LTS compared to the HTS.

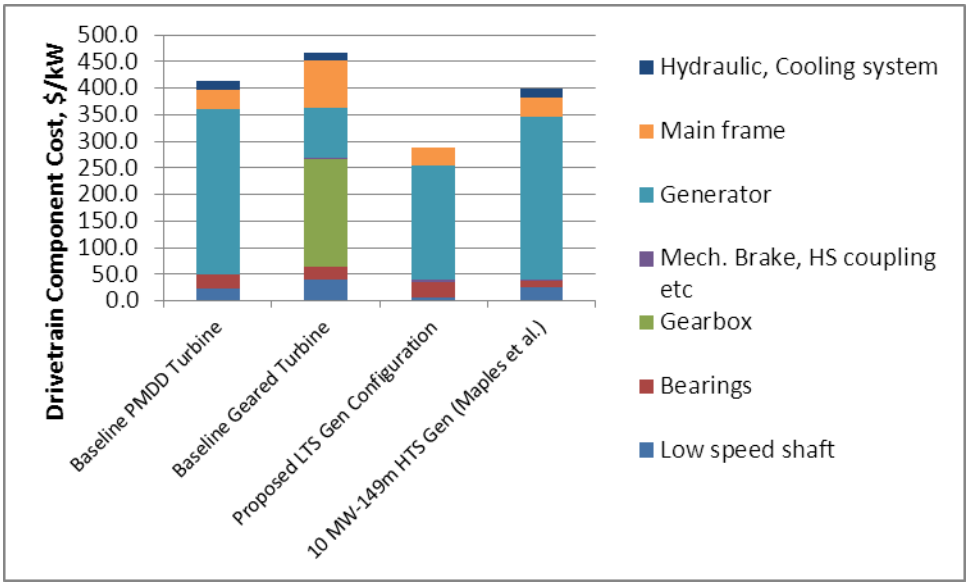


Figure 28 – Comparison of Drivetrain Component Costs

Additional reductions in COE are available at this large turbine size through complementary technologies focusing on the rotor cost and loads the turbine creates (i.e. blade mass/cost reduction technologies, advanced control strategies). These complementary technologies are most impactful when combined with this proposed drivetrain innovation. Even further reductions are possible with increased system reliability.

## 1.2.2.2 Calculation of Impact

As stated in section 1.2.2.1, the baseline (comparison) turbines and wind plant operating parameters (Table 1 of the attached COE calculation) are based on the example operating parameters of the 5 MW baseline in the RFP. The only exception to this baseline was the assumption of a jacket style foundation. A jacket was chosen since the water depth of 30m is near the transition point from monopile to jacket and for comparison purposes because a monopile would be cost prohibitive at the proposed configuration of 10 MW. Therefore, both the baselines (PMDD and geared) and proposed configuration would have the same foundation type. The proposed configuration with the LTS generator technology allows the drivetrain to cost-effectively scale to 10MW. In order to keep the other turbine components cost-effective, the rotor diameter was increased only to 160m, thereby increasing the specific power of the proposed turbine to 0.5 kW/m$^2$ from 0.4 kW/m$^2$. This increase in specific power occurs since a lower cost generator allows the optimization of the specific power to be less sensitive to the turbine rating. Since the rotor diameter increased, the hub height was also increased to maintain a constant clearance from the bottom of the rotor to the ocean level. The increase in hub height results in an increase in average wind speed by 1.7% based on the base wind shear. The maximum rotor Cp was unchanged across all of the configurations. Finally, in order to provide a clear example of the benefit from LTS generator, 10 MW PMDD and geared configurations were also added to the data tables.

The turbine capital cost and balance of system (BOS) cost data are summarized in Table 2 of the COE calculation attachment in Appendix D. The base turbine capital cost data in the attached COE analysis is

based on both the Fingersh et al. [2] and the Maples et al. [1] reports. Specifically the Maples et al. [1] is used primarily for the drivetrain components and some of the BOS components while the Fingersh et al [2] is used for the majority of the rest of the turbine. The Fingersh et al. [2] data was updated to 2010 dollars via an algorithm to escalate component costs to alternate dollar year bases using Producer Price Indices at the manufactured component level. This method of escalating the cost is consistent with Maples et al. [1]. The data from this model was found to be representative of current offshore wind turbines when calculated in terms of constant, 2010 dollars, and including the marinization cost adder. The cost for the LTS generator was established by creating a bill of material for the proposed generator.

Fingersh et al. [2] was found to insufficiently model the costs of the foundation, installation, and electrical collection portions of the offshore BOS costs, and instead Maples et al. [1] provided a reference point at 3.6MW at which a GE-internal model was used to scale these costs. This model calculates a savings (in $/kW) for the proposed configuration foundation due to the higher specific power (less swept area per kW). Additionally for the 10MW proposed configuration, cost reductions are calculated for the installation and electrical collection due to the reduced number of installation sites and reduced length of inter-array collection cables, respectively. The Maples et al. [1] was used for the “transportation”, “port and staging equipment”, and “other” portions of the BOS costs. The resulting initial capital cost is reduced by 17% from the proposed LTS direct drive generator configuration compared to the baseline.

The O&M and LRC costs (Tables 3 & 4 of the attached COE calculation in Appendix D assume that the proposed concept has an equivalent maintenance and mean time between failures as current PMDD architectures. Both the baseline O&M and LRC costs are obtained from Fingersh et al. [2] updated to 2010 dollars in the same method above using the Producer Price Indices. The reduction in the O&M cost for the proposed design is based on two reductions. First, a portion of the O&M cost is directly a function of the number of turbines and is independent of the turbine cost. This cost can be thought of as the cost to access a turbine, such as the availability of access and installation equipment along with the labor associated with the servicing. Secondly, the parts and consumables for the O&M are slightly cheaper in $/kW, resulting in a further reduction. Both of these items together reduce the O&M by almost 24%. The LRC for the proposed design is reduced through a less expensive component for the proposed design in $/kW, specifically the generator. This reduction in LRC is estimated at 13%.

The proposed power curve (Table 5 of the attached COE calculation in Appendix D) includes the LTS generator efficiency estimates as determined during Phase 1 of the current project. Figure 29 compares the drivetrain efficiencies (including transformer, cabling, and converter losses) incorporating these full and part-load LTS generator efficiencies along with data from Maples et al. [1] for PMDD and geared turbines. The proposed power curve also includes the effect of the increase in specific power, which changes the AEP (annual energy production). The output AEP is calculated based on a Rayleigh wind distribution based on the wind speed at hub height and weibull K factor listed in Table 1 of the attached COE calculation in Appendix D. The resulting total AEP (Table 6 of the attached COE calculation) is the electrical power output at the bus bar for a given turbine. Included in this total AEP are losses from blade soiling, controls, drivetrain mechanical, and drivetrain electrical system losses. Additional losses due to collection, transmission, and other wind plant interactions are assumed to be 10% and do not change based on the proposed design. Additionally, since the assumptions are that there is no change to the mean time between failures or mean time to repair between the compared options, the availability is consistent with that of PMDD configurations.

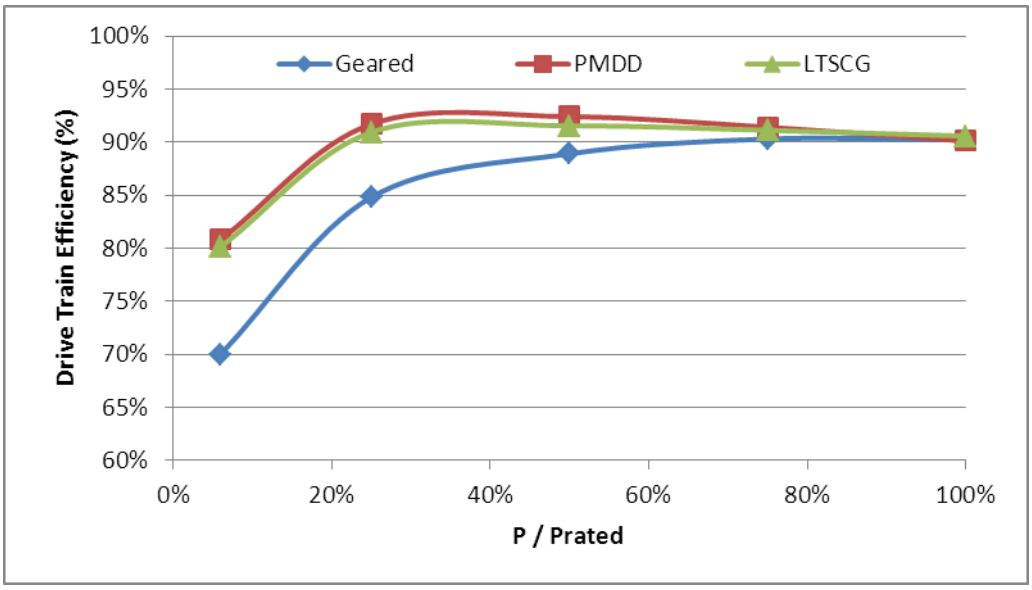


Figure 29 – Drive Train Efficiencies Used to Calculate Turbine Power Curve

The COE summary (Table 7 of the attached COE calculation Appendix D) is calculated based on the assumptions, justifications, calculations, and sources above along with the process defined in the Request for Proposal.

### 1.2.2.3 Impact on Integrated System

In our concept, the major drivetrain unreliability, the gearbox, has been removed, and the cryogenic system should not add appreciably to unreliability, based on experience in the MRI industry, which we are borrowing in our concept. The brushes we have added to the rotating armature have a wear-out life which we estimate to be at least 5 years at these slow rotation speeds, so they can easily be checked and replaced as needed annually. Finally, the normal wear out of the field winding in a generator, which is expected in all utility generators over their 20-30 year life and is due to thermal excursions during operation, should be absent in our LTS field, which is held at constant temperature.

For the wind farm system as a whole, the compact, lightweight nature of our LTS concept allows the largest wind generator power outputs possible. This has the general scaling benefit of reducing the number of turbines for any given wind farm size. This in turn decreases part counts, interconnections, and repair visits (as outlined above) and thereby improves overall farm reliability.

## 1.2.3 Performance / Cost Tradeoff Analysis

Since the key differentiator for the proposed concept is through a decrease in the capital cost of the generator, it makes sense to further optimize the LTS generator design to decrease cost. One such way was already discussed earlier in the report by optimizing the length of LTS wire required. Another way is to optimize the number of poles the generator has for the lowest cost weight. The current design has 36 poles and the analysis was completed with this constraint. If the design has less poles, the SC wire length needed will drop while the mass of the generator will increase. Since from Table 19, the LTS wire is the dominant portion of the cost, there may be some room left for optimization of the number of poles.

The impact the number of poles has on the cost of the LTS wire and the weight of the armature core was also investigated. Decreasing the number poles increases the armature core weight but reduces the SC

wire cost. Just by reducing the number of poles to 30, the LTS wire cost reduces by 18%. GRC expects to optimize the number of poles for the lowest cost generator (or drivetrain system) in subsequent follow on work.

Another trade analyzed is the use of composite non-magnetic armature teeth for potential weight and cost reduction. The overall size and performance including efficiency and thermal are essentially the same for the non-magnetic teeth configuration as compared to the magnetic (baseline). The core yoke depth decreases and more space has to be allotted to the coils versus the teeth, so that weight is shifted from the core to the coils.

The use of non-magnetic teeth reduces the mass of the armature frame and core assembly by 4 metric metric tonnes. This is done by reducing the core punchings weight by over 10 metric tonnes. Some of this advantage is removed with the heavier coils with insulation as well as the addition of the composite teeth. The coils with insulation are not just heavier, they are also much more expensive as it is very likely that Litz wire coils would have to be used to minimize circulating losses. This increase in cost outweighs any potential weight benefit. Therefore, magnetic teeth were used throughout the conceptual design described in this report.

## 1.3 SOPO Task Number 1.3 - Identification of high-risk components

### 1.3.1 Failure Modes and Effects Analysis

A full Failure Modes and Effects Analysis (FMEA) regarding the performance of the generator was carried out and a summary of the results is shown below. The following FMEA process was used:

1. For each failure mode, list the possible plant/unit effects assuming protection devices/logic fail to prevent the failure from "going too far."
2. Rate the Severity of each potential effect. How significant is the impact of the effect to the customer?
3. List the potential causes of the failure mode including failure of the protection device/logic as a cause.
4. Rate the Likelihood of Occurrence of each cause.
5. For each potential cause, list the main method for preventing the cause from occurring, detecting that the cause has occurred and/or preventing the failure from continuing to the point that the effects are realized.
6. Rate the Merit of the preventative measures. How well do the preventative measures prevent or detect a cause and prevent it from continuing to the point that failure effects will be realized.
7. To calculate the Risk Priority Number (RPN), pick the highest rated effect that is a logical outcome of each cause (if more than one effect) and multiply that 'Severity' by the 'Likelihood of Occurrence' and the 'Merit of Preventative Measures'.
8. For any cause where the RPN is greater than 120, recommend actions to eliminate the cause and/or enhance the prevention and detection.

The identified risks have been grouped into four key areas and have been summarized in Figure 30 below.

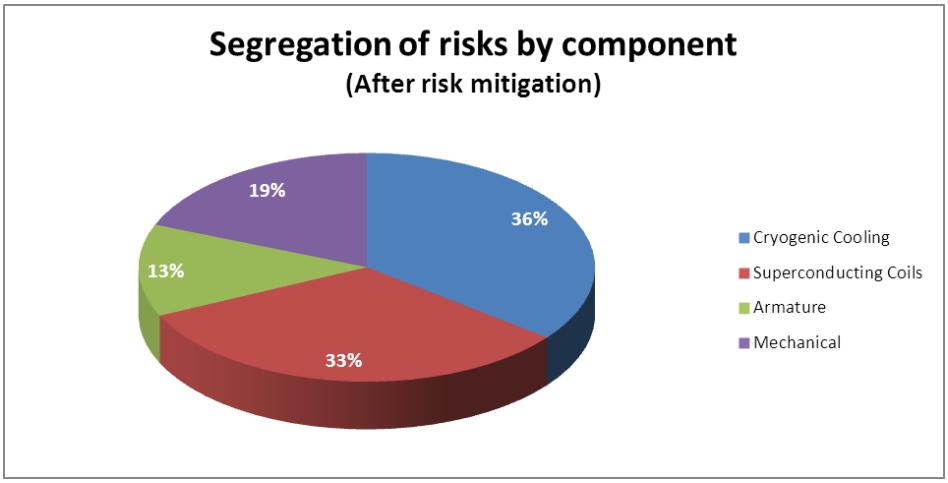


Figure 30 – Segregation of Risks

The cryogenic cooling aspects and superconducting coils pose the highest risk areas. Further analysis of the cumulative Risk Priority Numbers is shown below both before and after risk mitigation. The

Cumulative RPN is simply a summation of all the RPNs for each individual identified risk and provides a top level view of the potential effect of the suggested risk mitigation activities.

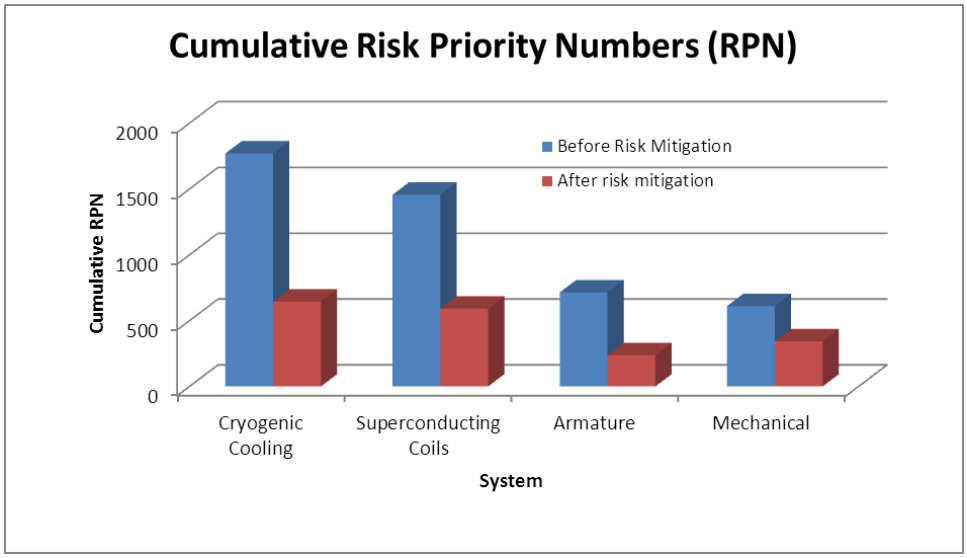


Figure 31 – Cumulative Risk Priority Numbers

A more detailed analysis of the individual risks is provided in the following sets of figures. It should be noted that the FMEA dealt with the complete generator including all conventional components. Therefore, some of the risks identified below will also be common to more conventional wind turbine generators. These particular risks will be identified below and will not necessarily need to be addressed as part of any further ongoing investigations. Any further investigations should therefore only concentrate on mitigating risks that are particular to the transformational technology being proposed here.

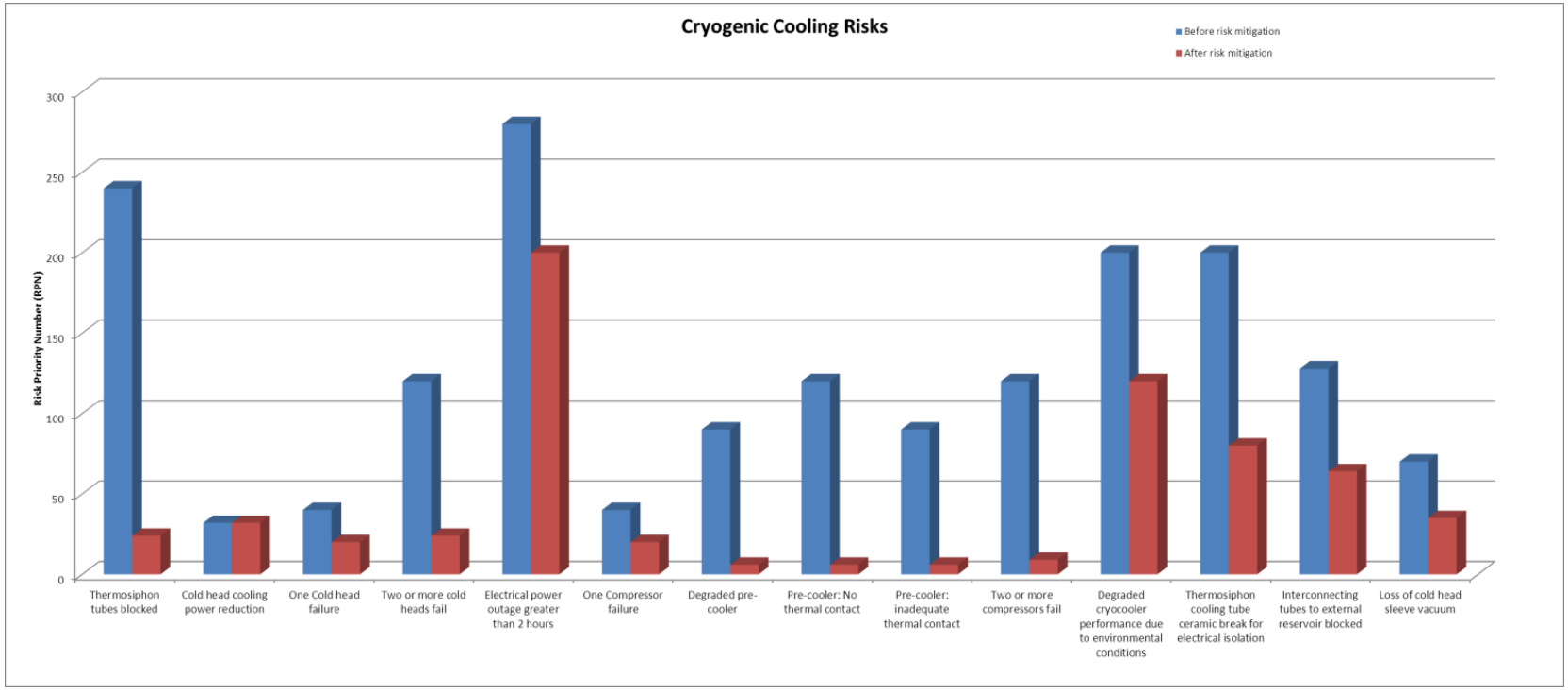


Figure 32 – Cryogenic Cooling Risks

A key reliability risk has been eliminated by not having to use a cryogen transfer coupling for our concept generator design.

One of the highest risks identified concerns the loss of electrical power to the nacelle which lasts more than 2 hours. During this power outage, the cryocoolers and compressors will not be functioning and the superconducting coils will start to warm up. However, due to the large thermal mass available, there will be sufficient time to detect this power failure and de-energize the superconducting coils safely providing that sufficient back-up power is available for the monitoring, diagnostic and control equipment. If the power outage was less than 2 hours, the cryogenic thermal mass would still be sufficiently cold to allow rapid re-cooling to bring the generator back to its normal operating condition.

The next three highest risks associated with the cryogenic cooling system relate to the environmental conditions that the equipment must work within (i.e. up-tower off-shore where vibration, temperature extremes and salinity are all present), a ceramic component that is used to join parts of the cryogenic cooling circuit and blockage of the cryogenic cooling tubes.

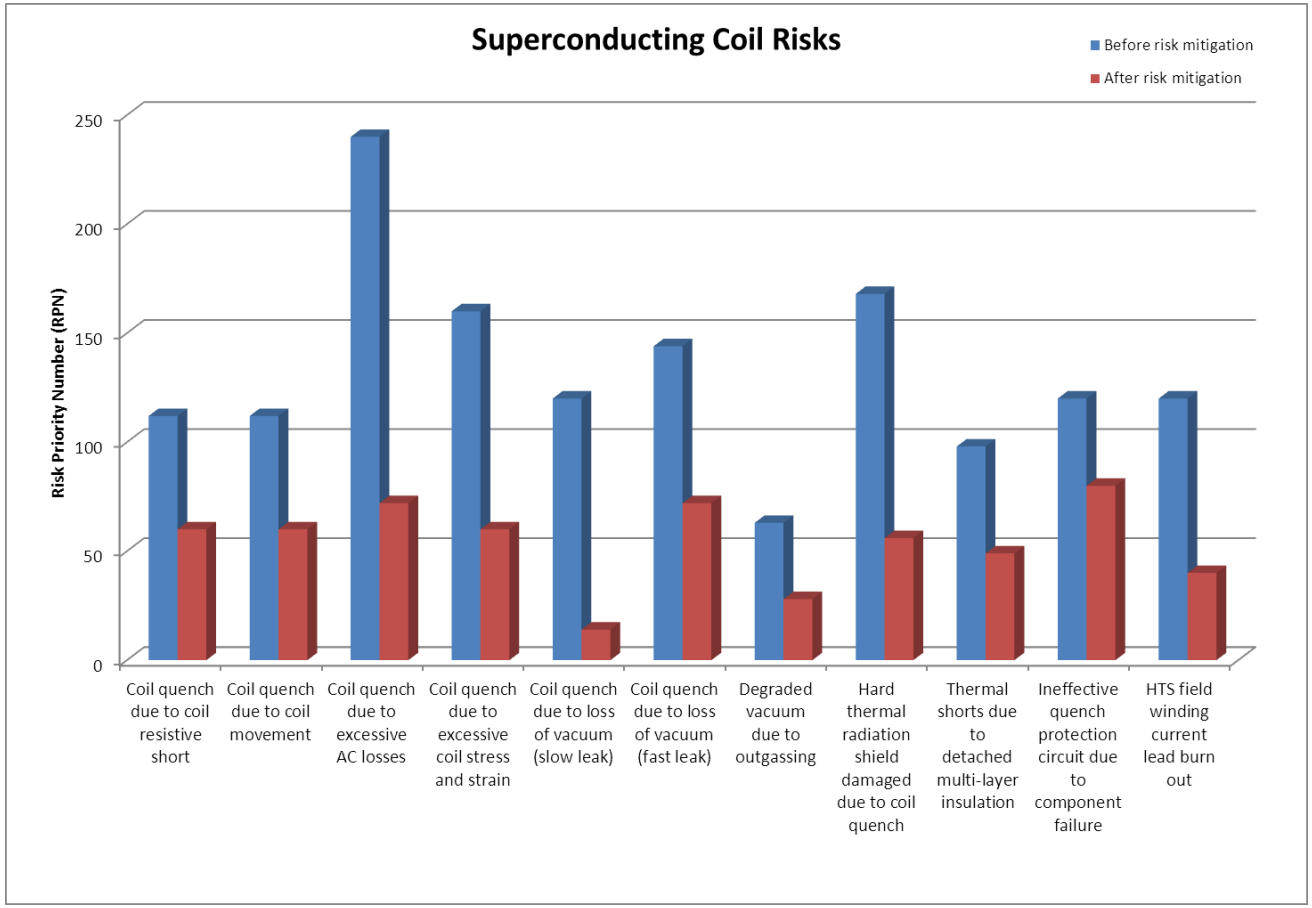


Figure 33 – Superconducting Coil Risks

The level of A.C. losses within the superconducting field coils is a clear risk and is not well understood in general and even less so under the very different operating conditions experienced by an off-shore wind turbine generator of this power rating. Other risks relate primarily to coil quench due to excessive stress, strain, heat loads and ineffective quench protection and current leads.

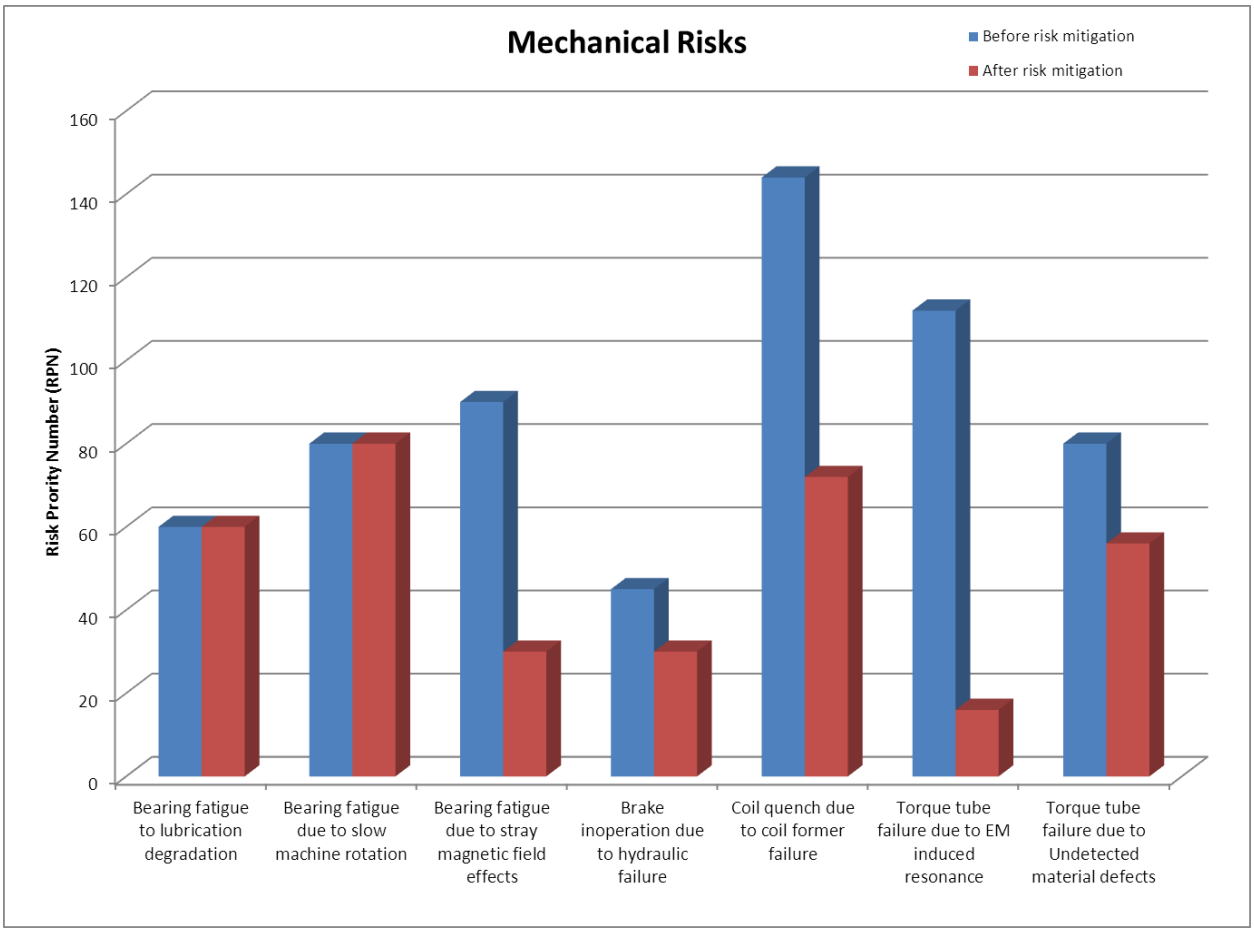


Figure 34 – Mechanical Risks

The risks related to bearing and mechanical brake issues are common to other more conventional wind turbine generators and will not necessarily need to be dealt with in any further ongoing investigations. However, the possible detrimental effects on bearings due to stray magnetic fields should be investigated further. Issues related to the torque tube and former design should also be addressed.

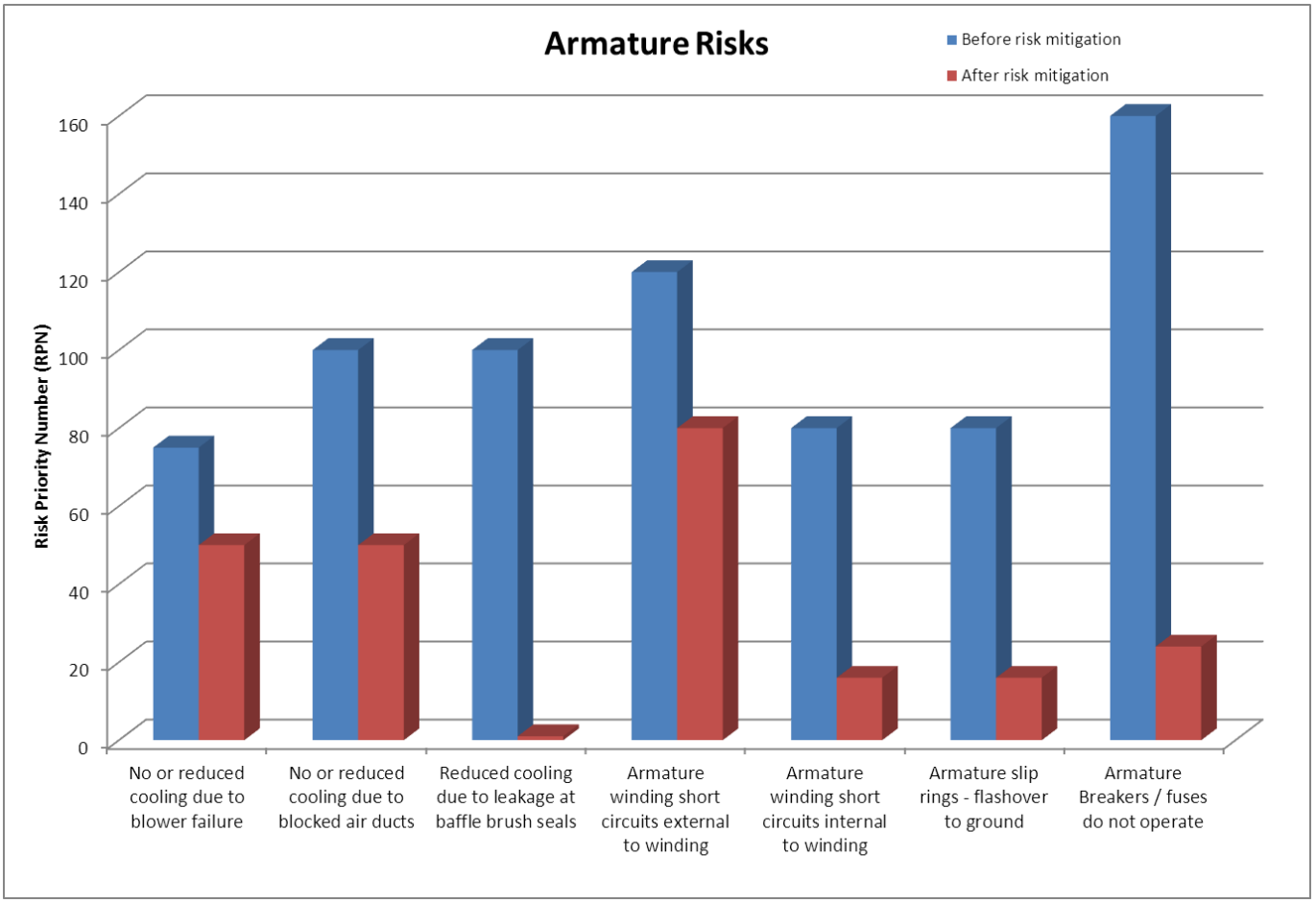


Figure 35 – Armature Risks

The original design for the armature air-cooling circuit required the use of baffles and brush seals to maintain closure of the air-path. However, movement over time causes the seals to leak. By opting to move the air-blowers to a different position on the generator (below the field winding assembly) as shown in some of the earlier pictures, the need for baffles and seals was removed and the associated risk eliminated.

With regards to short circuits external to the generator – i.e. close to the generator terminals, the cause will most likely be due to a fault within the convertor. Due to the low generator reactances associated with this type of superconducting machine design, the short circuit currents and associated torques can be very high. One mitigation activity would be to include protection circuitry within the convertor itself which is most likely a new development activity for the convertor manufacturer. Another potential solution would be re-designing the superconducting generator to have higher reactances. Unfortunately, this usually results in a heavier machine but should not be ruled out at this stage – a compromise has to be made between machine weight and machine survivability during a major fault event.

This page intentionally left blank

# 2. SOPO Task Number 2 Project Management and Reporting

This is a continuous process throughout the entire project phase.

**Team Meetings**
GE-Global Research (GE-GR) team meetings were held every two weeks to report on progress and to present the latest developments on each allocated task. A review panel consisting of a Chief Scientist, Chief Engineer and Laboratory Manager would be present at these meetings to review the design and analysis work. In addition to this review panel, experts from other laboratories at GE-GR and other relevant GE businesses (e.g. Wind and Healthcare) were called upon to either review particular work packages or to carry out further analyses.

Additional meetings were held to address issues as and when they arose on an ad hoc basis. The entire GE-GR team was co-located at the Niskayuna site and this provided for an extremely positive team dynamic and supported improved communication between team members. Oak Ridge National Laboratory was also involved for key meetings, e.g. Failure Modes and Effects Analysis, review of A.C. Loss calculations, Phase 2 risk-mitigation test plans.

**Project Plan**
A top-level Project Plan was defined at the start of the project and this provided a framework for the various key design activities as well as the approximated allocated hours for each key team member. This plan was intentionally made flexible to accommodate for changes in resource level and activity throughout the project period.

**Master Task Action List**
A Master Task Action List was maintained to drive and monitor critical tasks assigned to individual team members.

**Reports**
Webinar reports were provided to the Department of Energy on a monthly basis and written reports and financial statements were provided quarterly.

**Post Project Review**
A Post Project Review session is being planned after the completion of Phase 1 of the project to review 'lessons learnt' and to address 'areas for improvement' – from a team working and project management perspective.

# 3. Commercialization Plan

This transformational LTS superconducting wind turbine generator presents an outstanding commercialization opportunity which can also reduce US dependence on energy imports and rare earth materials from foreign sources and increase US jobs. Of course, it is imperative that a convincing business case be developed. It is obviously a plus that this is a 'green' technology with greatly reduced energy-related emissions, but it must compete with all other alternatives within whatever regulatory regimes are in place. That is why building larger wind turbines with lower COE (cost of energy), such as this technology allows, is important.

As the largest manufacturer of wind turbines in the Western Hemisphere, GE is in an ideal position to take commercial advantage of this cutting edge technology. GE Global Research (GEGR) must, has, and will continue to work carefully with the GE Wind business to carry forward the commercialization strategy of this technology. The GE Wind business knows what is important for commercialization, and the most

important single factor in judging this (or any) new wind technology is projected COE. GEGR is using both the COE method outlined in the DOE FOA (to report to the DOE) as well as an internal proprietary LCOE (levelized cost of energy) methodology developed and approved by GE Wind (for communication with GE Wind) to do these calculations, and current projections have been carried out based on accumulated work and information to date and reported here. These models contain all the expected factors (capital costs, operating and maintenance costs, performance), and they look favorable. Many cost/performance tradeoffs have been carried out for these calculations, and many more will be needed before a best prototype can be established. Perhaps the second most important factor is projected reliability of the new system. Unreliability of the new system in excess of the experience with current wind turbines can quickly degrade any projected COE advantage. A new technology as transformative as an LTS wind turbine will get particular scrutiny in this area, both from the GE Wind and from potential wind customers. The most effective way to prove the reliability case sufficiently to all parties is to demonstrate prototypes running in the field with no more than the projected/expected reliability issues.

GE's technology and product development process includes an NTI (new technology introduction) and NPI (new product introduction) phase. The LTS wind generator is now in the NTI phase and will be there until approximately TRL 6 (i.e., running a prototype in the field). This Phase 1 contract places us in TRL 3, with a design and critical analyses complete. Phase 2 of this contract will place us in TRL 4, with critical subsystem experimental validations. During prototype construction (TRL 5-6), GE Wind will gradually become more involved in the GEGR work. GE will probably seek to continue partnering with DOE in the high-risk prototype (NTI) phase. At about TRL 6, if the technical and market factors are favorable, the development will enter the NPI phase, and GE Wind will take over most of the work to carry the technology to TRL 9 (full commercialization), with consultation as needed from GEGR.

GE Wind has, of course, an established supply chain for most common parts of GE wind turbines. Other parts (e.g., blades, tower structures) must be scaled up from existing technology to accommodate these much larger turbines, and the cost/benefit of these required developments must also figure into any commercialization decision at 10 MW and higher. GE and its vendors have the capability to deal with these scale-ups. The entirely new (for wind) portion of our LTS wind generator is the superconducting part. GE Healthcare owns a factory in Florence, SC, which manufactures all its LTS MRI (magnetic resonance imaging) magnets for global consumption. This factory has the capacity and capability to manufacture the LTS portions of our LTS wind generator, which are generally less demanding in magnetic performance than the MRI magnets. Therefore, GE Wind has a clear "line-of-sight" to the supply chain for an LTS wind generator.

There must be a clear strategy and commercial case to take this forward. At this writing, most of the interest in very large offshore wind turbines is within Europe. We are hopeful that the combination of technology improvement, cost reduction, and policy will enable a large offshore wind market in the US in the near future. However, GE is uniquely positioned because we are not constrained by the development of the US market in order for this technology to provide value. The wind business is a global business, and GE responds to it as such, not just from a US-centric point of view. The ultimate commercialization of this technology is not solely reliant upon the deployment of US offshore turbines, as there is another avenue of benefit in US manufacturing jobs for providing this equipment overseas.

# Appendix A – Concept Design Description

A conceptual design has been completed for a direct drive 10MW superconducting wind turbine generator employing low temperature superconductors for the field winding. In order to keep production costs low for such machines, conventional technology and production techniques have been used wherever possible.

The armature (outer assembly) rotates while the superconducting field winding (inner assembly) is stationary.

The armature core will be of conventional laminated iron construction while the armature winding uses conventionally insulated copper strip conductors. The iron yoke (back iron) of the armature incorporates cooling holes and the entire armature is cooled using several axially oriented air-blowers. The armature is cantilevered and rotates at the same speed as the turbine blades.

Electrical power is transferred from the rotating armature to static convertors using a set of high-power transfer slip rings and carbon brushes.

The convertors are full power convertors rated for 10MW and are water-cooled.

A braking system is employed on the rotating armature.

Two main sets of bearings are employed – a tapered X-type bearing and a roller bearing and have been sized to manage extreme wind loads.

The field winding assembly consists of a total of 36 superconducting racetrack coils wound using low temperature superconducting (LTS) wire. These racetrack coils are wound on aluminum coil formers, potted in epoxy-resin and located in slots machined out of an annular aluminum former structure. The coils are held in place with bolted aluminum closure plates. An aluminum thermal radiation shield surrounds the field coil assembly and the complete assembly is housed within an aluminum vacuum chamber. The field winding assembly is also cantilevered and is stationary.

A two-part torque tube supports the superconducting field winding assembly and allows the transmission of torque from the field winding to the tower support structure while minimizing the heat loads between the cryogenically cold field winding and structures at ambient temperature.

Cooling tubes carrying a low volume of helium liquid are embedded within the body of the annular field coil former and allow the superconducting coils and the former to be cooled to 4.2Kelvin.These cooling tubes are connected to small reservoirs located at either end of the vacuum chamber. The reservoirs collect gaseous helium from the cooling tubes. The gaseous helium is then recondensed by the second stage of a set of cryocoolers inserted within the reservoirs. The first stage of the cryocoolers provides cooling to the thermal radiation shield. The cryocoolers are located within sleeves which allow for easy maintenance and swap-out if necessary.

The cryocoolers have associated compressors which can be either air or water cooled. The cryocoolers, compressors and helium conduction tubes form a complete closed loop with no loss of helium during operation.

An additional more powerful cryocooler will be used for the initial cool down of the field winding from ambient temperature to some intermediate cryogenic temperature. Once this intermediate temperature is reached, this cryocooler will be withdrawn and the cooling process will continue using the other cryocoolers described above.

The field coils and associated cryogenically cold structures will be monitored using temperature sensors and a GE developed monitoring system. This monitoring system will, in turn, operate a field coil protection system in the unlikely event of a quench (i.e. superconducting coils transitioning from their superconducting state to their normal and highly resistive state).

# Appendix B – Concept Design Specifications

| GENERATOR ELECTROMAGNETIC DESIGN | | |
|---|---|---|
| **Generator** | | |
| Rated Power | 10 MW | |
| Rated Speed | 10 rpm | |
| Rated Voltage | 3300 V line-line | |
| Rated Current | 1750 A | |
| Rated Power Factor | 1.0 | |
| Full load shaft torque | 10 MNm | |
| Full Load Efficiency | 95-96% | |
| Armature Core Outer Diameter | 4.83 m | |
| Armature Core Length | 1.88 m | |
| Armature core inner diameter | 4.34 m | |
| Armature winding total axial length | 2.66 m | |
| Field Assembly Outer Diameter | 4.29 m | |
| Physical Air gap length | 19 mm | |
| No. of poles / No. of slots | 36 | 648 |
| Armature Winding Type | 3 phase, 2 layer, lap, form wound | |
| Armature Winding Insulation | Class F (with Class B temperature rise) | |
| Armature core laminations (material / lamination thickness) | Silicon steel, M47 | 24 gauge (0.025 inches) |
| Core and winding impregnation | Resin vacuum pressure impregnation (VPI) | |
| Superconducting Field Coil Ampere-Turns | 928000 AT/pole | |
| Field Pole Center flux density | 3.5 T | |
| Air gap, peak flux density | 2.6 T | |
| Armature teeth flux density | 3.0 – 3.4 T | |
| Armature yoke (back of iron) flux density | 2.5 T | |
| Generator weight | 145 metric tons (potential to reduce to 135 metric tons) | |
| Shear Stress | 179 kPa | |
| Torque Density (EM only) | 197 Nm/kg | |
| Torque Density (Drivetrain) | 92 Nm/kg | |
| Transient reactance, Xd | 0.09 p.u. | |
| Sub-transient reactance, X”d | 0.07 p.u. | |
| | | |
| **Generator Fault Protection** | | |
| Protection system | Set of fusible elements located in an bath of dielectric coolant (Patent application dated 12.23.2009 (GB2464024) filed by GE – Power Conversion (formerly Converteam, UK) | |
| | | |
| **Armature Slip Rings** | | |
| No. of slip rings | 4 | |
| Slip ring material | Steel | |
| Slip ring outer diameter | 3 m | |
| No. of carbon brushes per slip ring | 30 | |
| Current per brush | 60 A | |

| | | |
|---|---|---|
| Rotational speed | 10 rpm | |
| Brush wear per year | less than 2mm @ 10 rpm | |
| Total operational loss @ 10MW | 4.6kW | |
| | | |
| **Armature Cooling** | | |
| Cooling | Axial air cooled through air gap and cooling holes in yoke (back iron) | |
| Axial cooling holes | 2 rows of cooling holes, 0.625 inches diameter | |
| Maximum allowable armature winding hot spot temperature | 130$^{o}$C | |
| No. of air blowers (Total No. / Redundant No.) | 6 | 2 |
| Air blower model | Aerovent Model 15-BIUB-2815-5 Belt Drive Utility Blower. | |
| Electrical power input for 6 blowers | 39 kW | |
| | | |
| **Power Convertors** | | |
| Convertor type | Full power 4-Quadrant | |
| Model type | General Electric MV7000 series, 12MVA, 3.3kV, water-cooled pulse width modulation (PWM) inverter with press-pack IGBTs | |
| | | |
| **SUPERCONDUCTING COIL DESIGN** | | |
| Coil type | Racetrack | |
| Coil width | 35.00 mm | |
| Coil height | 101.60 mm | |
| Coil length straight | 1879.60 mm | |
| Coil Inner Width | 261.01 mm | |
| End radius | 124.58 mm | |
| Type of conductor used | Cu-(NbTi), Supercon Inc.(Part No. SC-VSF-SSCI-1.0mm | |
| Bare diameter of conductor | 1.00 mm | |
| Insulated diameter of conductor | 1.05 mm | |
| Number of filaments | 7400 | |
| Filament diameter | 7.5 micron | |
| Insulation | Formvar | |
| Operating current | 276.86 A | |
| Total ampere turns | 928000 AT | |
| Maximum field in the coil | 7.35 T | |
| Critical current at the maximum field | 466.75 A | |
| Short sample percentage | 59.96 % | |
| Critical temperature | 6.08 K | |
| Stored energy of the system | 40.6 MJ | |
| Inductance of all the coils | 1059 H | |
| Total conductor used for 36coils | 720 km | |
| Total estimated weight of the coils | 3840 kg | |
| | | |
| **Quench Protection** | | |
| Type | Passive system with back-to-back diodes, resistors and quench-back film heaters. | |
| | | |

| | | |
|---|---|---|
| **Field Winding Power Supply** | | |
| Voltage | 64 Vdc min | |
| Current | 335 Adc min | |
| Model | GE Ex2100e (rated for up to 600Vac input and 500 Adc output). Full wave silicon controlled rectifier bridge with positive and negative forcing. | |
| | | |
| **CRYOGENIC COOLING AND VACUUM DESIGN** | | |
| **Field coil assembly** | | |
| Temperature (Superconducting Coils) | 4.3 K | |
| Temperature (Thermal Shield) | 42 K | 45 K max |
| **Cryocoolers** | | |
| RDK 415 dual-stage (No. of units: 4) 1st stage / 2nd stage | 40 K | 4.3 K |
| AL 600 coolers (No. of units: 2) | Cool down / event | |
| **Cooling performance** | | |
| Total heat loads (1st / 2nd stage) | 125.6 W | 4.84 W |
| **Transients and events** | | |
| Cool down time | 7 ½ days | |
| Cool down time thermal shield | 6 days | |
| End temperature after quench | 58 K | |
| Re-cool back to operating temperature | 21 ½ hours | |
| Ride-through time[1] (all coolers off) | 3 hours | |
| **3-Phase short circuit** | | |
| Field winding assembly warm up, time | 140 ms | |
| Field winding assembly heat load in 140 ms | 40 kJ | |
| | | |
| **MECHANICAL DESIGN** | | |
| **Armature and Field Support** | | |
| Hub Moment (Nominal / Extreme) | 5.8e9 N-mm | $5.1x10^{10}$ N-mm |
| EM Radial load (Nominal / Extreme) | 160 psi | 160 psi + $5.5x 10^{6}$ N/in*air gap delta closedown |
| EM Torque (Nominal / Extreme) | 9.554e9 N-mm | $2.7x10^{10}$ N-mm |
| Armature and field support structure type | Cantilevered, conic | |
| Shaft type (Yield Stress) | 380 MPa | |
| Field support structure (stress under extreme torque load / safety factor) | 177 MPa | >2 |
| Armature support structure (stress under extreme torque load / safety factor) | < 100 MPa | > 3 |
| | | |
| Gravity Only (air gap closedown / max. equivalent stress) | 0.9 mm (5%) | 20 MPa (19.0 SF) |
| Gravity, Nom. Wind (air gap closedown / max. equivalent stress) | 1.7 mm (9%) | 35 MPa (10.9 SF) |
| Gravity, Nom. Wind, EM (air gap closedown / max. equivalent | 2.3 mm (12%) | 37 MPa (10.3 |

[1] Depending on reservoir size, currently 13 liter)

| | | |
|---|---|---|
| stress) | | SF) |
| Gravity, Extreme Wind, EM (air gap closedown / max. equivalent stress) | 7.8 mm (41%) | 287 MPa (1.3 SF) |
| | | |
| **Bearings** | | |
| Front bearing (i.e. towards hub-end) | Double row tapered roller bearing | |
| Back bearing (i.e. towards non hub-end) | Floating cylindrical bearing | |
| Bearing span | 1350 mm | |
| Lubrication | Greased (auxiliary cooling or oil systems not required) | |
| Lubrication interval | 6 – 12 months (typical for main bearings of existing wind turbines) | |
| Bore Diameter (mm) | 1800 mm | 1800 mm |
| Outer Diameter (mm) | 2500 mm | 2400 mm |
| Width (mm) | 750 mm | 500 mm |
| Dynamic Capacity (kN) | 40,000 kN | 25,000 kN |
| Static Capacity (kN) | 122,000 kN | 66,000 kN |
| Estimated Life (hrs) | 370,000 hours | 415,000 hours |
| | | |
| **Brakes** | | |
| Type | Hydraulically actuated calipers with brake pads and shear locking pin | |
| Brake disc diameter | 3700 mm | |
| No. of calipers | 4 to 8 | |
| | | |
| **Field Winding Assembly** | | |
| Outer vacuum chamber (Material / safety factor under extreme load and gravity) | Al 6061-T6 | > 9 |
| Thermal shield (Material / safety factor under extreme load and gravity) | Al 1100 | > 6 |
| Upper torque tube (Material / safety factor under extreme load and gravity) | TiAl6V4 | > 2 |
| Lower torque tube (Material / safety factor under extreme load and gravity) | TiAl6V4 | > 5 |
| Coil former (Material / safety factor under extreme load and gravity) | Al A356-T61 | > 4 |
| Torque tube buckling factor (under extreme load condition) | 1.5 (4.5x electromagnetic nominal torque) | |
| Outer vacuum chamber wall thickness | 16 mm | |
| Thermal shield wall thickness | 8 mm | |
| | | |
| **Torque Tube Bolt design** | | |
| Bolt type / Material | M24 | Inconel |
| No. of bolts | 100 | |
| Load | $1.366 \times 10^7$ N | |
| Safety factor | 1.3 | |
| | | |
| **COST OF ENERGY** | | |
| Cost of energy reduction potential | 13 to 18% reduction compared to PMDD 5 MW baseline | |
| COE | 0.075 $/kWh | |
| | | |

| Turbine and Wind Plant Operating Parameters | |
|---|---|
| Wind Plant Rating | 250 MW |
| Turbine Rating | 10 MW |
| Rotor Diameter | 160 m |
| Hub Height | 112.0 m |
| Distance to Shore | 25 km |
| Water Depth | 30 m |
| Wind Speed @ Hub Height | 10.2 (m/s) |
| Max Rotor Cp | 0.482 |
| Specific Power | 0.5 $kW/m^2$ |
| | |

# Appendix C - Technology Readiness Level Scale

**Source**: ARPA-E

| TRL | Description |
|---|---|
| 1 | *Basic principles observed and reported*<br>Scientific research begins with a systematic study directed toward greater knowledge or understanding of the fundamental aspects of phenomena and of observable facts without specific applications or products in mind. The knowledge or understanding will later be translated into applied RD&D. Example might include studies of a technology's basic properties. |
| 2 | *Technology concept and/or application formulated*<br>Invention begins. Once basic principles are observed, practical applications can be invented. Applications are speculative and there may be no proof or detailed analysis to support the assumptions. |
| 3 | *Analytical and experimental critical function and/or characteristic proof of concept.* Active R&D is initiated. This includes analytical studies and laboratory studies to physically validate analytical predictions of separate elements of the technology. Examples include components that are not yet integrated or representative. |
| 4 | *Component and/or breadboard validation in laboratory environment.* Basic technological components are integrated to establish that they will work together. This is relatively "low fidelity" compared to the eventual system. Examples include integration of "ad hoc" hardware in the laboratory. |
| 5 | *Component and/or breadboard validation in relevant environment.* Fidelity of breadboard technology increases significantly. The basic technological components are integrated with reasonably realistic supporting elements so it can be tested in a simulated environment. Examples include "high fidelity" laboratory integration of components. |
| 6 | *System/subsystem model or prototype demonstration in a relevant environment.*<br>Representative model or prototype system, which is well beyond that of TRL-5, is tested in a relevant environment. This represents a major step up in a technology's demonstrated readiness. Examples include testing a prototype in a high-fidelity laboratory environment or in simulated operational environment. |
| 7 | *System prototype demonstration in a operational environment.* It requires the demonstration of an actual system prototype in an operational environment, such as in a light duty vehicle on the road. Examples include testing a prototype battery in an operational hybrid gas-electric vehicle. |
| 8 | *Actual system completed and qualified through test and demonstration.* Technology has been proven to work in its final form and under expected conditions. Examples include developmental test and evaluation of the system in its intended parent system to determine if it meets design specifications. |
| 9 | *Actual system proven through successful mission operations.* The technology is applied and operated in its final form and under real life conditions, such as those encountered in operational test and evaluation. In almost all cases, this is the end of the last "bug fixing" aspects of true system development. Examples include using the system under various real life conditions. |

# Appendix D – Cost of Energy (COE) Calculations

**References**:

1. "Comparative Assessment of Direct Drive High Temperature Superconducting Generators in Multi-Megawatt Class Wind Turbines", B. Maples, M. Hand, and W. Musial, NREL/TP-5000-49086. National Renewable Energy Lab, October 2010.
2. "Wind Turbine Design Cost and Scaling Model", L. Fingersh, M. Hand, and A. Laxson; NREL/TP-500-40566. National Renewable Energy Lab, December 2006

| Description | Baseline PMDD Comparison | Baseline Geared Comparison | Scaled-up PMDD Comparison | Scaled-up Geared Comparison | Proposed LTS Gen Configuration |
|---|---|---|---|---|---|
| Wind Plant Rating (MW) | 250 | 250 | 250 | 250 | 250 |
| Number of Turbines | 50 | 50 | 25 | 25 | 25 |
| System Design Life (yrs.) | 20 | 20 | 20 | 20 | 20 |
| Turbine Rating (MW) | 5 | 5 | 10[(a)] | 10[(a)] | 10[(a)] |
| Rotor Diameter (m) | 126 | 126 | 160[(b)] | 160[(b)] | 160[(b)] |
| Hub Height (m) | 95 | 95 | 112[(c)] | 112[(c)] | 112[(c)] |
| Foundation Type | Jacket[(d)] | Jacket[(d)] | Jacket[(d)] | Jacket[(d)] | Jacket[(d)] |
| Distance to Shore (km) | 25 | 25 | 25 | 25 | 25 |
| Water Depth (m) | 30 | 30 | 30 | 30 | 30 |
| Wind Speed @ Hub Height (m/s) | 10.0 | 10.0 | 10.2[(e)] | 10.2[(e)] | 10.2[(e)] |
| Weibull K Factor | 2.0 | 2.0 | 2.0 | 2.0 | 2.0 |
| Base Wind Shear | 0.1 | 0.1 | 0.1 | 0.1 | 0.1 |
| Air Density (kg/m3) | 1.225 | 1.225 | 1.225 | 1.225 | 1.225 |
| Max Rotor Cp | 0.482 | 0.482 | 0.482 | 0.482 | 0.482 |
| Vcut-in (m/s) | 3 | 3 | 3 | 3 | 3 |
| Vcut-out (m/s) | 25 | 25 | 25 | 25 | 25 |
| Losses | 10% | 10% | 10% | 10% | 10% |
| Availability | 95% | 94.0%[(f)] | 95% | 94.0%[(f)] | 95% |

Table 1: Description of Operating Parameters for the Turbine & Wind Plant

Table 1 Notes: Input Source: DE-FOA-0000439

a) 10 MW turbine chosen to maximize proposed configuration COE reduction. The drivetrain cost difference between the proposed LTS generator and either PMDD or geared configurations is expected to increase as the turbine rating is increased in the 1 to 10 MW range. This increasing difference in the cost is consistent to high temperature superconducting generator results provided in Maples et al [1], although more pronounced in the current proposed LTS generator. Also, by increasing to 10 MW, the BOS, O&M, and LRC costs should also be reduced.
b) Rotor diameter of 160m specified to allow specific power of turbine to increase to 0.5 $W/m^2$ from 0.4 $W/m^2$. This increase in specific power specifies a lower swept area of the turbine, allowing for lower rotor costs and loads at the expense of reduced annual energy production.
c) Hub height is determined by keeping a constant clearance between the lower tip of the blade and the ground (in this case at 32m).
d) Transition from monopile to jacket foundations are expected to be needed at 30m water depth and with a rating of10 MW. For consistency between comparisons, all configurations incorporate a jacket style foundation.
e) Increased wind speed is due to the increased hub height and base wind shear with the equation; $U_{new} = U_{baseline}\ (\text{Hub Height}_{new} / \text{Hub Height}_{baseline})^{\text{Base Wind Shear}}$.
f) Geared availability is reduced by 1% due to an internal estimate of the additional downtime associated with planned and unplanned maintenance associated with gearboxes.

| **Turbine Capital Cost** | | | | | | | |
|---|---|---|---|---|---|---|---|
| ***Analysis Level*** | ***Representative Categories*** | ***Baseline PMDD Turbine ($/kW)*** | ***Baseline Geared Turbine ($/kW)*** | ***Scaled-up PMDD Comparison ($/kW)*** | ***Scaled-up Geared Comparison ($/kW)*** | ***Proposed* LTS Gen *Configuration ($/kW)*** | ***Component Weight (kg/kW)*** |
| **1** | ***Rotor:*** | ***240.5*** | ***240.5*** | ***231.0*** | ***231.0*** | ***231.0*** | ***14.2*** |
| 2 | Blades[(a)] | 163.1 | 163.1 | 162.1 | 162.1 | 162.1 | 8.9 |
| 2 | Hub[(a)] | 25.1 | 25.1 | 20.1 | 20.1 | 20.1 | 3.4 |
| 2 | Pitch mechanism & bearings[(a)] | 50.3 | 50.3 | 47.5 | 47.5 | 47.5 | 1.6 |
| 2 | Spinner, Nose Cone[(a)] | 2.0 | 2.0 | 1.4 | 1.4 | 1.4 | 0.2 |
| **1** | ***Drive train, nacelle:*** | ***637.0*** | ***690.9*** | ***738.0*** | ***741.0*** | ***490.4*** | ***32.9*** |
| 2 | Low speed shaft[(b)] | 22.9 | 39.5 | 39.5 | 39.3 | 6.4 | 1.4 |
| 2 | Bearings[(c)] | 25.8 | 25.8 | 29.9 | 29.9 | 30.0 | 1.7 |
| 2 | Gearbox[(d)] | | 202.2 | | 256.7 | | |
| 2 | Mech. Brake, HS coupling etc.[(c)] | 2.0 | 2.0 | 2.0 | 2.0 | 3.0 | 2 |
| 2 | Generator[(e)] | 309.9 | 92.7 | 393.5 | 92.7 | 215.9 | 11.1 |
| 2 | Variable speed electronics[(c)] | 101.2 | 101.2 | 101.2 | 101.2 | 80.0 | 0.8 |
| 2 | Yaw drive & bearing[(a)] | 35.4 | 35.4 | 35.9 | 35.9 | 35.9 | 2.9 |
| 2 | Main frame[(f)] | 36.6 | 89.0 | 33.1 | 80.5 | 33.1 | 13.6 |
| 2 | Electrical connections[(a)] | 71.9 | 71.9 | 71.9 | 71.9 | 71.9 | |
| 2 | Hydraulic, Cooling system[(c)] | 16.5 | 16.5 | 16.5 | 16.5 | 0.0 | |
| 2 | Nacelle cover[(a)] | 14.6 | 14.6 | 14.2 | 14.2 | 14.2 | 1.2 |
| **1** | ***Tower:*** [(a)] | ***152.3*** | ***152.3*** | ***144.3*** | ***144.3*** | ***144.3*** | ***60.8*** |
| N/A | Anchoring System | | | | | | |
| **1** | ***Control, Safety System, and Condition Monitoring***[(a)] | ***13.6*** | ***13.6*** | ***6.8*** | ***6.8*** | ***6.8*** | |

Table 2: Initial Capital Cost of Wind Energy Systems

| **Turbine Capital Cost Continued** | | | | | | | |
|---|---|---|---|---|---|---|---|
| ***Analysis Level*** | ***Representative Categories*** | ***Baseline PMDD Turbine ($/kW)*** | ***Baseline Geared Turbine ($/kW)*** | ***Scaled-up PMDD Comparison ($/kW)*** | ***Scaled-up Geared Comparison ($/kW)*** | ***Proposed* LTS Gen *Configuration ($/kW)*** | ***Component Weight (kg/kW)*** |
| **1** | ***Other:*** | ***308.9*** | ***325.1*** | ***334.0*** | ***334.9*** | ***259.7*** | |
| 2 | Marinization[(a)] (15.00% of Turbine and Tower System) | 154.5 | 162.6 | 167.0 | 167.5 | 129.9 | |
| 2 | Offshore Warranty Premium[(h)] (15.00% of Turbine & Tower System) | 154.5 | 162.6 | 167.0 | 167.5 | 129.9 | |

| **Balance of System Cost** | | | | | | |
|---|---|---|---|---|---|---|
| ***Analysis Level*** | ***Representative Categories*** | ***Baseline PMDD Turbine ($/kW)*** | ***Baseline Geared Turbine ($/kW)*** | ***Scaled-up PMDD Comparison ($/kW)*** | ***Scaled-up Geared Comparison ($/kW)*** | ***Proposed* LTS Gen *Configuration ($/kW)*** |
| **1** | ***Transportation:*** | **133.0** | **133.0** | **106.0** | **106.0** | **106.0** |
| 2 | Turbine[(g)] | 133.0 | 133.0 | 106.0 | 106.0 | 106.0 |
| 2 | Substation/Interconnection | Incl. | Incl. | Incl. | Incl. | Incl. |
| 2 | BOS Hardware | Incl. | Incl. | Incl. | Incl. | Incl. |
| **1** | ***Installation, Foundation & Electrical Interconnection[(g)(h)(i)]*** | **1242.2** | **1242.2** | **1007.6** | **1007.6** | **1007.6** |
| 2 | Foundation/Support Structure | Incl. | Incl. | Incl. | Incl. | Incl. |
| 2 | Port and Staging Equipment[(h)] | Incl. | Incl. | Incl. | Incl. | Incl. |
| 2 | Turbine Installation[(g)] | Incl. | Incl. | Incl. | Incl. | Incl. |
| 2 | Foundation Installation[(i)] | Incl. | Incl. | Incl. | Incl. | Incl. |
| 2 | Wind Plant Collection | Incl. | Incl. | Incl. | Incl. | Incl. |
| 2 | Substation | Incl. | Incl. | Incl. | Incl. | Incl. |
| 2 | Wind Plant / Grid Interconnection | Incl. | Incl. | Incl. | Incl. | Incl. |

Table 2 Continued: Initial Capital Cost of Wind Energy Systems

| **Balance of System Cost Continued** | | | | | | |
|---|---|---|---|---|---|---|
| ***Analysis Level*** | ***Representative Categories*** | ***Baseline PMDD Turbine ($/kW)*** | ***Baseline Geared Turbine ($/kW)*** | ***Scaled-up PMDD Comparison ($/kW)*** | ***Scaled-up Geared Comparison ($/kW)*** | ***Proposed* LTS Gen *Configuration ($/kW)*** |
| **1** | ***Other:*** | **217.7** | **219.6** | **212.6** | **212.7** | **204.0** |
| 2 | Permits, Engineering, Site Assessment[(h)] | 39.4 | 39.4 | 39.4 | 39.4 | 39.4 |
| 2 | Personal Access Equipment[(h)] | 17.8 | 17.8 | 17.8 | 17.8 | 17.8 |
| 2 | Scour Protection[(h)] | 83.3 | 83.3 | 83.3 | 83.3 | 83.3 |
| 2 | Surety Bond (Decommissioning - 3.0% if ICC)[(h)] | 77.2 | 79.1 | 72.0 | 72.1 | 63.5 |

Table 2 Continued: Initial Capital Cost of Wind Energy Systems

Table 2 Notes

a) Blades, hub, pitch mechanism & bearings, spinner / nose cone, yaw drive & bearing, electrical connections, nacelle cover, tower, controls / safety system / condition monitoring, and marinization mass and cost estimates were obtained by using equations from Fingersh et al. [2] updated to 2010 dollars (from 2002 dollars) using Producer Price Indices published by the U.S. Department of Labor.

b) PMDD low speed shaft mass and cost calculated from equation developed from data reported in Maples et al. [1] with rotor diameter as the variable. Geared low speed shaft cost determined from equation in Fingersh et al. [2] updated to 2010 dollars (from 2002 dollars) using Producer Price Indices published by the U.S. Department of Labor (also consistent with Maples et al. [1]). Proposed LTSCG low speed shaft mass and cost from Phase 1 design analysis summarized in the LTS generator BOM.

c) PMDD and geared bearings, mechanical brake / HS coupling, variable speed electronics, and hydraulic / cooling system mass and cost estimates were obtained by using equations from Fingersh et al. [2] updated to 2010 dollars (from 2002 dollars) using Producer Price Indices published by the U.S. Department of Labor. Proposed LTS generator bearings, mechanical brake / HS coupling, variable speed electronics mass and cost from Phase 1 design analysis summarized in the LTS generator BOM. Proposed LTS generator hydraulics / cooling system included in generator mass and cost.

d) Baseline geared gearbox mass and cost were obtained by using equations from Fingersh et al. [2] updated to 2010 dollars (from 2002 dollars) using Producer Price Indices published by the U.S. Department of Labor (also consistent with Maples et al. [1]). Scaled-up geared gearbox mass and cost scaled linearly with torque from baseline gearbox mass and cost. Resulting cost is similar to result from Maples et al. [1].

e) PMDD generator mass obtained by using equation from Maples et al. [1]. Baseline PMDD generator cost was obtained by using equations from Fingersh et al. [2] updated to 2010 dollars (from 2002 dollars) using Producer Price Indices published by the U.S. Department of Labor (also consistent with Maples et al. [1]). Scaled PMDD generator cost scaled linearly from calculated generator mass. Geared generator mass and cost determined from equations in Fingersh et al. [2] updated to 2010 dollars (from 2002 dollars) using Producer Price Indices published by the U.S. Department of Labor (also consistent with Maples et al. [1]). Proposed LTS generator mass and cost from Phase 1 design analysis summarized in the LTS generator BOM.

f) Main frame mass and cost calculated from equations developed from data reported in Maples et al. [1] with rotor diameter as the variable. Proposed LTS generator assumed to have same main frame mass as the PMDD although lower LTS generator mass may allow lighter and cheaper main frame.

g) Foundation / support structure (including anchoring system), turbine transportation, turbine installation, and electrical interconnection estimated from 3.6 MW reference point from Appendix A of Maples et al. [1] and scaled based on internal GEGR offshore BOS model. Foundation cost includes transition from reference point of monopole to current study of jacket foundations.

h) Offshore warranty premium, port & staging equipment, permits / engineering / site assessment, personal access equipment, scour protection, and surety bond costs estimated from 3.6 MW reference point from Appendix A of Maples et al. [1].

i) Foundation installation costs calculated directly from internal GEGR offshore BOS model. Foundation costs reference point reported in Maples et al. [1] appears to be too low to include installation cost. Therefore, separate foundation installation cost added.

| **Operations & Maintenance Cost** | | | | | | |
|---|---|---|---|---|---|---|
| ***Analysis Level*** | ***Representative Categories*** | ***Baseline PMDD Turbine ($/kW/yr.)*** | ***Baseline Geared Turbine ($/kW/yr.)*** | ***Scaled-up PMDD Comparison ($/kW/yr.)*** | ***Scaled-up Geared Comparison ($/kW/yr.)*** | ***Proposed* LTS Gen *Configuration ($/kW/yr.)*** |
| 1 | General Maintenance[(a)] | 120.3 | 130.5 | 92.6 | 100.3 | 89.9 |
| 1 | Bottom Lease[(b)] | 6.5 | 6.4 | 6.1 | 6.0 | 6.1 |
| 1 | Plant Operations Cost | | | | | |
| 1 | Scheduled Turbine Maintenance (labor, parts, and supplies) | | | | | |
| 1 | Unscheduled Turbine Maintenance (labor, parts, and supplies) | | | | | |
| 1 | Equipment & Facilities Maintenance (labor, parts, and supplies) | | | | | |
| 1 | Administration and support | | | | | |

Table 3: Operations and Maintenance Costs of Wind Energy Systems

Table 3 Notes

a) Baseline turbine general maintenance costs were obtained by using equations from Fingersh et al. [2] updated to 2010 dollars (from 2002 dollars) using Producer Price Indices published by the U.S. Department of Labor. Baseline geared cost increased by 10% over PMDD to incorporate higher O&M costs associated with gearboxes. Scaled-up cost based on internal GEGR O&M model that includes a portion of the cost as a function of the number of turbines, project size, turbine capital cost, and BOS cost.

b) Bottom lease costs were obtained by using equations from Fingersh et al. [2] updated to 2010 dollars (from 2002 dollars) using Producer Price Indices published by the U.S. Department of Labor.

| **Levelized Replacement Cost** | | | | | | |
|---|---|---|---|---|---|---|
| ***Analysis Level*** | ***Representative Categories*** | ***Baseline PMDD Turbine ($/kW/yr.)*** | ***Baseline Geared Turbine ($/kW/yr.)*** | ***Scaled-up PMDD Comparison ($/kW/yr.)*** | ***Scaled-up Geared Comparison ($/kW/yr.)*** | ***Proposed* LTS Gen *Configuration ($/kW/yr.)*** |
| 1 | Blades | | | | | |
| 1 | Electrical Collection | | | | | |
| 1 | Drivetrain | | | | | |
| 1 | Other | | | | | |
| 1 | Unknown[(a)] | 20.8 | 24.1 | 22.4 | 24.7 | 17.4 |

Table 4: Levelized Replacement Costs of Wind Energy Systems

Table 4 Notes

a) Baseline turbine general maintenance costs were obtained by using equations from Fingersh et al. [2] updated to 2010 dollars (from 2002 dollars) using Producer Price Indices published by the U.S. Department of Labor. Baseline geared cost increased by an additional 10% over PMDD to incorporate higher O&M costs associated with gearboxes. Proposed LTS generator assumed to have identical failure rate as PMDD and therefore LRC cost is directly dependent on turbine capital cost.

| | | Baseline PMDD Comparison | | | Baseline Geared Comparison | | |
|---|---|---|---|---|---|---|---|
| **Bin** | **V (m/s)** | **P[(a)] (kW)** | **Cp[(b)]** | **AEP (kWh)** | **P[(a)] (kW)** | **Cp[(b)]** | **AEP (kWh)** |
| 1 | 0.5 | 0 | 0.000 | 0 | 0 | 0.000 | 0 |
| 2 | 1 | 0 | 0.000 | 0 | 0 | 0.000 | 0 |
| 3 | 1.5 | 0 | 0.000 | 0 | 0 | 0.000 | 0 |
| 4 | 2 | 0 | 0.000 | 0 | 0 | 0.000 | 0 |
| 5 | 2.5 | 0 | 0.000 | 0 | 0 | 0.000 | 0 |
| 6 | 3 | 83 | 0.482 | 14877 | 47 | 0.482 | 8372 |
| 7 | 3.5 | 144 | 0.482 | 29636 | 105 | 0.482 | 21501 |
| 8 | 4 | 213 | 0.482 | 49109 | 170 | 0.482 | 39208 |
| 9 | 4.5 | 304 | 0.482 | 77011 | 257 | 0.482 | 65067 |
| 10 | 5 | 419 | 0.482 | 114734 | 367 | 0.482 | 100467 |
| 11 | 5.5 | 574 | 0.482 | 167010 | 516 | 0.482 | 150014 |
| 12 | 6 | 774 | 0.482 | 236104 | 709 | 0.482 | 216221 |
| 13 | 6.5 | 991 | 0.482 | 313480 | 919 | 0.482 | 290820 |
| 14 | 7 | 1241 | 0.482 | 402708 | 1163 | 0.482 | 377543 |
| 15 | 7.5 | 1524 | 0.482 | 503007 | 1442 | 0.482 | 475889 |
| 16 | 8 | 1843 | 0.482 | 613110 | 1759 | 0.482 | 584916 |
| 17 | 8.5 | 2198 | 0.482 | 730798 | 2114 | 0.482 | 702744 |
| 18 | 9 | 2582 | 0.482 | 851813 | 2502 | 0.482 | 825328 |
| 19 | 9.5 | 2976 | 0.482 | 967001 | 2905 | 0.482 | 943911 |
| 20 | 10 | 3347 | 0.482 | 1064027 | 3285 | 0.482 | 1044228 |
| 21 | 10.5 | 3693 | 0.482 | 1141008 | 3641 | 0.482 | 1124829 |
| 22 | 11 | 4032 | 0.481 | 1203022 | 3990 | 0.481 | 1190340 |
| 23 | 11.5 | 4298 | 0.465 | 1231067 | 4266 | 0.465 | 1221705 |
| 24 | 12 | 4517 | 0.425 | 1234536 | 4493 | 0.424 | 1228025 |
| 25 | 12.5 | 4689 | 0.376 | 1215951 | 4673 | 0.375 | 1211747 |
| 26 | 13 | 4818 | 0.334 | 1178777 | 4808 | 0.334 | 1176331 |
| 27 | 13.5 | 4867 | 0.298 | 1117383 | 4860 | 0.298 | 1115705 |
| 28 | 14 | 4933 | 0.268 | 1057098 | 4929 | 0.267 | 1056281 |
| 29 | 14.5 | 4974 | 0.241 | 989627 | 4973 | 0.241 | 989335 |
| 30 | 15 | 4995 | 0.218 | 917836 | 4994 | 0.217 | 917791 |

Table 5: Turbine Power Curve and Site Specific Wind Speed

| | | Baseline PMDD Comparison | | | Baseline Geared Comparison | | |
|---|---|---|---|---|---|---|---|
| Bin | V (m/s) | P[(a)] (kW) | Cp[(b)] | AEP (kWh) | P[(a)] (kW) | Cp[(b)] | AEP (kWh) |
| 31 | 15.5 | 5000 | 0.197 | 844426 | 5000 | 0.197 | 844426 |
| 32 | 16 | 5000 | 0.179 | 772166 | 5000 | 0.179 | 772166 |
| 33 | 16.5 | 5000 | 0.163 | 702614 | 5000 | 0.163 | 702614 |
| 34 | 17 | 5000 | 0.149 | 636219 | 5000 | 0.149 | 636219 |
| 35 | 17.5 | 5000 | 0.137 | 573329 | 5000 | 0.137 | 573329 |
| 36 | 18 | 5000 | 0.126 | 514199 | 5000 | 0.126 | 514199 |
| 37 | 18.5 | 5000 | 0.116 | 458995 | 5000 | 0.116 | 458995 |
| 38 | 19 | 5000 | 0.107 | 407806 | 5000 | 0.107 | 407806 |
| 39 | 19.5 | 5000 | 0.099 | 360650 | 5000 | 0.099 | 360650 |
| 40 | 20 | 5000 | 0.092 | 317482 | 5000 | 0.092 | 317482 |
| 41 | 20.5 | 5000 | 0.085 | 278207 | 5000 | 0.085 | 278207 |
| 42 | 21 | 5000 | 0.079 | 242688 | 5000 | 0.079 | 242688 |
| 43 | 21.5 | 5000 | 0.074 | 210751 | 5000 | 0.074 | 210751 |
| 44 | 22 | 5000 | 0.069 | 182199 | 5000 | 0.069 | 182199 |
| 45 | 22.5 | 5000 | 0.064 | 156815 | 5000 | 0.064 | 156815 |
| 46 | 23 | 5000 | 0.060 | 134371 | 5000 | 0.060 | 134371 |
| 47 | 23.5 | 5000 | 0.057 | 114632 | 5000 | 0.057 | 114632 |
| 48 | 24 | 5000 | 0.053 | 97365 | 5000 | 0.053 | 97365 |
| 49 | 24.5 | 5000 | 0.050 | 82338 | 5000 | 0.050 | 82338 |
| 50 | 25 | 5000 | 0.047 | 69328 | 5000 | 0.047 | 69328 |
| 51 | 25.5 | 0 | 0.000 | 0 | 0 | 0.000 | 0 |
| 52 | 26 | 0 | 0.000 | 0 | 0 | 0.000 | 0 |
| 53 | 26.5 | 0 | 0.000 | 0 | 0 | 0.000 | 0 |
| 54 | 27 | 0 | 0.000 | 0 | 0 | 0.000 | 0 |
| 55 | 27.5 | 0 | 0.000 | 0 | 0 | 0.000 | 0 |
| 56 | 28 | 0 | 0.000 | 0 | 0 | 0.000 | 0 |
| 57 | 28.5 | 0 | 0.000 | 0 | 0 | 0.000 | 0 |
| 58 | 29 | 0 | 0.000 | 0 | 0 | 0.000 | 0 |
| 59 | 29.5 | 0 | 0.000 | 0 | 0 | 0.000 | 0 |
| 60 | 30 | 0 | 0.000 | 0 | 0 | 0.000 | 0 |

Table 5 Continued: Turbine Power Curve and Site Specific Wind Speed

| | | Scaled-up PMDD Comparison | | | Scaled-up Geared Comparison | | | Proposed LTS Gen Configuration | | |
|---|---|---|---|---|---|---|---|---|---|---|
| **Bin** | **V (m/s)** | **P[(a)] (kW)** | **Cp[(b)]** | **AEP (kWh)** | **P[(a)] (kW)** | **Cp[(b)]** | **AEP (kWh)** | **P[(a)] (kW)** | **Cp[(b)]** | **AEP (kWh)** |
| 1 | 0.5 | 0 | 0.000 | 0 | 0 | 0.000 | 0 | 0 | 0.000 | 0 |
| 2 | 1 | 0 | 0.000 | 0 | 0 | 0.000 | 0 | 0 | 0.000 | 0 |
| 3 | 1.5 | 0 | 0.000 | 0 | 0 | 0.000 | 0 | 0 | 0.000 | 0 |
| 4 | 2 | 0 | 0.000 | 0 | 0 | 0.000 | 0 | 0 | 0.000 | 0 |
| 5 | 2.5 | 0 | 0.000 | 0 | 0 | 0.000 | 0 | 0 | 0.000 | 0 |
| 6 | 3 | 102 | 0.482 | 17572 | 32 | 0.482 | 5551 | 146 | 0.482 | 25235 |
| 7 | 3.5 | 200 | 0.482 | 39829 | 125 | 0.482 | 24937 | 241 | 0.482 | 48020 |
| 8 | 4 | 310 | 0.482 | 69605 | 230 | 0.482 | 51629 | 348 | 0.482 | 77988 |
| 9 | 4.5 | 457 | 0.482 | 112788 | 370 | 0.482 | 91272 | 490 | 0.482 | 120842 |
| 10 | 5 | 645 | 0.482 | 171653 | 549 | 0.482 | 146114 | 671 | 0.482 | 178818 |
| 11 | 5.5 | 896 | 0.482 | 253771 | 789 | 0.482 | 223483 | 915 | 0.482 | 259303 |
| 12 | 6 | 1219 | 0.482 | 362982 | 1100 | 0.482 | 327481 | 1230 | 0.482 | 366266 |
| 13 | 6.5 | 1572 | 0.482 | 485902 | 1440 | 0.482 | 445212 | 1574 | 0.482 | 486655 |
| 14 | 7 | 1978 | 0.482 | 628423 | 1834 | 0.482 | 582707 | 1971 | 0.482 | 626418 |
| 15 | 7.5 | 2440 | 0.482 | 789554 | 2285 | 0.482 | 739335 | 2425 | 0.482 | 784779 |
| 16 | 8 | 2961 | 0.482 | 967552 | 2796 | 0.482 | 913783 | 2939 | 0.482 | 960258 |
| 17 | 8.5 | 3543 | 0.482 | 1159689 | 3372 | 0.482 | 1103811 | 3514 | 0.482 | 1150428 |
| 18 | 9 | 4183 | 0.482 | 1361581 | 4011 | 0.482 | 1305508 | 4152 | 0.482 | 1351208 |
| 19 | 9.5 | 4906 | 0.482 | 1576305 | 4742 | 0.482 | 1523881 | 4876 | 0.482 | 1566794 |
| 20 | 10 | 5616 | 0.482 | 1769553 | 5463 | 0.482 | 1721442 | 5588 | 0.482 | 1760790 |
| 21 | 10.5 | 6322 | 0.482 | 1940905 | 6184 | 0.482 | 1898555 | 6297 | 0.482 | 1933418 |
| 22 | 11 | 7050 | 0.482 | 2096086 | 6929 | 0.482 | 2060095 | 7030 | 0.482 | 2090098 |
| 23 | 11.5 | 7679 | 0.479 | 2197600 | 7577 | 0.479 | 2168539 | 7663 | 0.479 | 2193198 |
| 24 | 12 | 8237 | 0.464 | 2256250 | 8156 | 0.464 | 2233836 | 8227 | 0.464 | 2253296 |
| 25 | 12.5 | 8716 | 0.444 | 2271953 | 8653 | 0.444 | 2255507 | 8709 | 0.444 | 2270209 |
| 26 | 13 | 9110 | 0.414 | 2247659 | 9064 | 0.414 | 2236270 | 9107 | 0.412 | 2246850 |
| 27 | 13.5 | 9325 | 0.370 | 2166072 | 9290 | 0.370 | 2157890 | 9323 | 0.368 | 2165623 |
| 28 | 14 | 9565 | 0.332 | 2080934 | 9541 | 0.331 | 2075759 | 9565 | 0.330 | 2080910 |
| 29 | 14.5 | 9743 | 0.299 | 1974928 | 9728 | 0.298 | 1971951 | 9744 | 0.297 | 1975154 |
| 30 | 15 | 9865 | 0.270 | 1854024 | 9857 | 0.269 | 1852541 | 9867 | 0.268 | 1854351 |

Table 5 Continued: Turbine Power Curve and Site Specific Wind Speed

| | | Scaled-up PMDD Comparison | | | Scaled-up Geared Comparison | | | Proposed LTS Gen Configuration | | |
|---|---|---|---|---|---|---|---|---|---|---|
| **Bin** | **V (m/s)** | **P[(a)] (kW)** | **Cp[(b)]** | **AEP (kWh)** | **P[(a)] (kW)** | **Cp[(b)]** | **AEP (kWh)** | **P[(a)] (kW)** | **Cp[(b)]** | **AEP (kWh)** |
| 31 | 15.5 | 9942 | 0.245 | 1723751 | 9939 | 0.244 | 1723170 | 9944 | 0.243 | 1724051 |
| 32 | 16 | 9985 | 0.222 | 1589158 | 9984 | 0.222 | 1589030 | 9986 | 0.221 | 1589339 |
| 33 | 16.5 | 10000 | 0.203 | 1454164 | 10000 | 0.202 | 1454164 | 10000 | 0.202 | 1454164 |
| 34 | 17 | 10000 | 0.185 | 1322285 | 10000 | 0.185 | 1322285 | 10000 | 0.184 | 1322285 |
| 35 | 17.5 | 10000 | 0.170 | 1196739 | 10000 | 0.170 | 1196739 | 10000 | 0.169 | 1196739 |
| 36 | 18 | 10000 | 0.156 | 1078100 | 10000 | 0.156 | 1078100 | 10000 | 0.155 | 1078100 |
| 37 | 18.5 | 10000 | 0.144 | 966771 | 10000 | 0.144 | 966771 | 10000 | 0.143 | 966771 |
| 38 | 19 | 10000 | 0.133 | 863003 | 10000 | 0.133 | 863003 | 10000 | 0.132 | 863003 |
| 39 | 19.5 | 10000 | 0.123 | 766906 | 10000 | 0.123 | 766906 | 10000 | 0.122 | 766906 |
| 40 | 20 | 10000 | 0.114 | 678467 | 10000 | 0.114 | 678467 | 10000 | 0.113 | 678467 |
| 41 | 20.5 | 10000 | 0.106 | 597567 | 10000 | 0.106 | 597567 | 10000 | 0.105 | 597567 |
| 42 | 21 | 10000 | 0.098 | 523998 | 10000 | 0.098 | 523998 | 10000 | 0.098 | 523998 |
| 43 | 21.5 | 10000 | 0.092 | 457479 | 10000 | 0.092 | 457479 | 10000 | 0.091 | 457479 |
| 44 | 22 | 10000 | 0.086 | 397669 | 10000 | 0.085 | 397669 | 10000 | 0.085 | 397669 |
| 45 | 22.5 | 10000 | 0.080 | 344185 | 10000 | 0.080 | 344185 | 10000 | 0.080 | 344185 |
| 46 | 23 | 10000 | 0.075 | 296616 | 10000 | 0.075 | 296616 | 10000 | 0.074 | 296616 |
| 47 | 23.5 | 10000 | 0.070 | 254528 | 10000 | 0.070 | 254528 | 10000 | 0.070 | 254528 |
| 48 | 24 | 10000 | 0.066 | 217484 | 10000 | 0.066 | 217484 | 10000 | 0.066 | 217484 |
| 49 | 24.5 | 10000 | 0.062 | 185044 | 10000 | 0.062 | 185044 | 10000 | 0.062 | 185044 |
| 50 | 25 | 10000 | 0.058 | 156779 | 10000 | 0.058 | 156779 | 10000 | 0.058 | 156779 |
| 51 | 25.5 | 0 | 0.000 | 0 | 0 | 0.000 | 0 | 0 | 0.000 | 0 |
| 52 | 26 | 0 | 0.000 | 0 | 0 | 0.000 | 0 | 0 | 0.000 | 0 |
| 53 | 26.5 | 0 | 0.000 | 0 | 0 | 0.000 | 0 | 0 | 0.000 | 0 |
| 54 | 27 | 0 | 0.000 | 0 | 0 | 0.000 | 0 | 0 | 0.000 | 0 |
| 55 | 27.5 | 0 | 0.000 | 0 | 0 | 0.000 | 0 | 0 | 0.000 | 0 |
| 56 | 28 | 0 | 0.000 | 0 | 0 | 0.000 | 0 | 0 | 0.000 | 0 |
| 57 | 28.5 | 0 | 0.000 | 0 | 0 | 0.000 | 0 | 0 | 0.000 | 0 |
| 58 | 29 | 0 | 0.000 | 0 | 0 | 0.000 | 0 | 0 | 0.000 | 0 |
| 59 | 29.5 | 0 | 0.000 | 0 | 0 | 0.000 | 0 | 0 | 0.000 | 0 |
| 60 | 30 | 0 | 0.000 | 0 | 0 | 0.000 | 0 | 0 | 0.000 | 0 |

Table 5 Continued: Turbine Power Curve and Site Specific Wind Speed

Table 5 Notes: Methodology from DE-FOA-0000439

a) Power is electrical power at the bus bar. Projected performance is calculated from a GEGR internal tool incorporating the drivetrain efficiencies in Figure xc, state-of-the-art control strategy, and the aero Cp.
b) Cp listed is the projected aero Cp at different wind speeds. The reduction of Cp at high wind speeds is due to blade pitching.

| Representative Categories | *Baseline PMDD Turbine* | *Baseline Geared Turbine* | *Scaled-up PMDD Comparison* | *Scaled-up Geared Comparison* | Proposed LTS Gen Configuration |
|---|---|---|---|---|---|
| Total Installed Capacity (MW) | 250 | 250 | 250 | 250 | 250 |
| AEPtot (MWh/y) | 1228865 | 1211745 | 1148097 | 1129677 | 1147452 |
| EL (total losses %) | 10% | 10% | 10% | 10% | 10% |
| Availability (%) | 95% | 94% | 95% | 94% | 95% |
| AEPnet (MWh/y) | 1050680 | 1025136 | 981623 | 955707 | 981071 |
| Capacity Factor: AEPnet/(Rated Power*8760 hours) | 48.0% | 46.8% | 44.8% | 43.6% | 44.8% |

Table 6: Annual Energy Wind Farm Production Summary

Table 6 Notes: Methodology from DE-FOA-0000439

| Representative Categories | Baseline PMDD Turbine ($/kWh) | Baseline Geared Turbine ($/kWh) | Scaled-up PMDD Comparison ($/kWh) | Scaled-up Geared Comparison ($/kWh) | Proposed LTS Gen Configuration ($/kWh) |
|---|---|---|---|---|---|
| Turbine Capital Cost | 0.0393 | 0.0418 | 0.0420 | 0.0433 | 0.0347 |
| Balance of System Cost | 0.0238 | 0.0244 | 0.0217 | 0.0223 | 0.0215 |
| Operations & Maintenance Cost | 0.0181 | 0.0200 | 0.0151 | 0.0167 | 0.0147 |
| Levelized Replacement Cost | 0.0049 | 0.0059 | 0.0057 | 0.0065 | 0.0044 |
| ***Total System:*** | 0.0861 | 0.0921 | 0.0845 | 0.0887 | 0.0753 |

Table 7: Wind Energy COE Summary

Table 7 Notes: Methodology from DE-FOA-0000439

This page intentionally left blank